Novel Role of Endothelial CD45 in Regulating Endothelial-to-Mesenchymal Transition in Atherosclerosis

Qianman Peng [1†], Kulandaisamy Arulsamy [2†], Yao Wei Lu[1,2], Hao Wu[1], Bo Zhu[1], Bandana Singh[1], Kui Cui[1], Jill Wylie-Sears,[1] Kathryn Li[1], Scott Wong[1], Douglas B. Cowan[1], Masanori Aikawa[3], Da-Zhi Wang[4], Joyce Bischoff[1*], Kaifu Chen[2*], Hong Chen[1*]

1. Vascular Biology Program, Boston Children's Hospital and Department of Surgery, Harvard Medical School; Boston, MA, 02115, USA.
2. Department of Cardiology, Boston Children's Hospital, Harvard Medical School; Boston, MA, USA.
3. Brigham and Women's Hospital, Harvard Medical School; Boston, MA, 02115, USA.
4. Center for Regenerative Medicine and USF Health Heart Institute, Department of Internal Medicine, University of South Florida, Tampa

†These authors contributed equally to this work.

***Correspondence to:** kaifu.chen@childrens.harvard.edu,
joyce.bischoff@childrens.harvard.edu
hong.chen@childrens.harvard.edu

Novel Role of Endothelial CD45 in Regulating Endothelial-to-Mesenchymal Transition in Atherosclerosis

Abstract:

Background: Protein-tyrosine-phosphatase CD45 is exclusively expressed in all nucleated cells of the hematopoietic system but is rarely expressed in endothelial cells. Interestingly, our recent study indicated that activation of the endogenous CD45 promoter in human endothelial colony forming cells (ECFCs) induced expression of multiple EndoMT marker genes. However, the detailed molecular mechanisms underlying CD45 that drive EndoMT and the therapeutic potential of manipulation of CD45 expression in atherosclerosis are entirely unknown.

Method: We generated a tamoxifen-inducible EC-specific CD45 deficient mouse strain (EC-iCD45KO) in an ApoE-deficient ($ApoE^{-/-}$) background and fed with a Western diet (C57BL/6) for atherosclerosis and molecular analyses. We isolated and enriched mouse aortic endothelial cells with CD31 beads to perform single-cell RNA sequencing. Biomedical, cellular, and molecular approaches were utilized to investigate the role of endothelial CD45-specific deletion in the prevention of EndoMT in $ApoE^{-/-}$ model of atherosclerosis.

Results: Single-cell RNA sequencing revealed that loss of endothelial CD45 inhibits EndoMT marker expression and transforming growth factor-β signaling in atherosclerotic mice. which is associated with the reductions of lesions in the $ApoE^{-/-}$ mouse model. Mechanistically, the loss of endothelial cell CD45 results in increased KLF2 expression, which inhibits transforming growth factor-β signaling and EndoMT. Consistently, endothelial CD45 deficient mice showed reduced lesion development, plaque macrophages, and expression of cell adhesion molecules when compared to $ApoE^{-/-}$ controls.

Conclusions: These findings demonstrate that the loss of endothelial CD45 protects against EndoMT-driven atherosclerosis, promoting KLF2 expression while inhibiting TGFβ signaling and EndoMT markers. Thus, targeting endothelial CD45 may be a novel therapeutic strategy for EndoMT and atherosclerosis.

Introduction:

Atherosclerotic cardiovascular disease is the leading cause of morbidity and mortality in the United States and most developed countries[1,2]. It is generally believed that endothelial dysfunction caused by the cholesterol and oxidized phospholipids in lipoproteins (ox-LDL) is one of the major initiating events[3]. Trapped lipoproteins activate endothelial cells and vascular smooth muscle cells to increase their expression of adhesion molecules and production of chemokines[4 5]. In turn, this leads to the recruitment of monocytes/lymphocytes into the arterial vessel wall[6]. Lesion progression involves the migration and proliferation of resident smooth muscle cells (SMCs)[2], extracellular matrix deposition[7], and lipid or necrotic core formation[8]. In advanced stages of atherosclerosis, increased endothelial dysfunction has been identified, and advanced plaque ruptures associated with thin, collagen-poor fibrous caps[9,10].

Endothelial-to-mesenchymal transition (EndoMT) is the process whereby an endothelial cell undergoes a series of molecular events that lead to progressively losing endothelial-specific markers and gaining mesenchymal phenotypes[11]. EndoMT plays a fundamental role in forming the cardiac valves of the developing heart, and mounting evidence indicates that EndoMT is involved in atherosclerosis[12-14]. ECs can be distinguished by the expression of cell–cell adhesion molecules, including platelet/EC adhesion molecule-1 (CD31/PECAM-1)[15], vascular endothelial (VE)-cadherin[16], tyrosine kinase with immunoglobulin-like and epidermal growth factor (EGF)-like domains 1 (TIE1), and TIE2[17,18]. During EndoMT, endothelial cells gain mesenchymal markers such as α-SMA[19], collagen[20], and SM22[21].

TGFβ signaling has been identified as the central player in driving EndoMT during atheroma progression [22], but the processes leading to activation of its signaling remain poorly defined. TGFβ-induced gene expression in ECs during EndoMT revealed induction of expression of a

number of pro-inflammatory chemokines and cytokines and their receptors[22], leucocyte adhesion molecules (such as ICAM-1 and VCAM-1)[23,24], pro-inflammatory extracellular matrix (ECM) component long linked to inflammation[7]. Endothelial phenotype and function can be maintained by FGFR signaling pathways that counter TGFβ-driven EndoMT during atherosclerosis [25,26]. A reduction in endothelial FGF-mediated signaling [27,28] or the primary FGF receptor in the endothelium (FGF receptor 1 [FGFR1]) activates TGFβ signaling, leading to EndoMT[29]. FGFR1's and transcriptional factor KLF2 expression in ECs is affected by certain inflammatory stimuli that induce a profound reduction in their expression[30].

Over the past few decades, findings indicated that CD45, a receptor-type protein tyrosine phosphatase, is exclusively expressed in all nucleated cells of the hematopoietic system except mature red blood cells and platelets. CD45, receptor type, C (*PTPRC*), was the prototypic receptor-like protein tyrosine phosphatase (PTP) and an essential regulator of signal transduction pathways in lymphocyte cells since it dephosphorylates, activating phospho-tyrosine sites and thereby dampening signaling pathways[31]. CD45 should rarely be expressed on endothelial cells. However, recent studies indicated that CD45 is expressed in umbilical vein endothelial cultures when stimulated with IL-1[32], and lung endothelial cells expressed both CD31 and CD45 in a pulmonary arterial hypertension rat model[33]. Importantly, we recently reported that activation of the endogenous CD45 promoter in human endothelial colony forming cells induced expression of EndoMT marker genes[34] Also, the CD45 phosphatase inhibitor blocked EndoMT activities in TGFβ1-treated ovine mitral valve endothelial cells[35]. However, whether endothelial CD45-specific deletion can prevent EndoMT-driven atherosclerosis remains entirely unknown. Thus, we propose that CD45 may also mediate EndoMT in atherosclerotic mouse models through new

mechanisms, highlighting that endothelial CD45 may be a new drug target for preventing or treating atherosclerosis.

Since we have reported that activation of the endogenous CD45 promoter in human endothelial colony forming cells induced migration, a hallmark of EndoMT, increased collagen gel contraction, a hallmark of mesenchymal cells, and decreased cell-cell barrier integrity, indicating reduced endothelial function[34]; it brings us the interest to uncover molecular mechanisms that CD45 drives EndoMT and promotes atherosclerotic progression. The principal objective of this study was to determine whether endothelial CD45-specific deletion could prevent EndoMT in atherosclerosis. To investigate the role of endothelial CD45 in EndoMT during atherosclerosis, we generated a tamoxifen-inducible EC-specific CD45-deficient mouse strain (EC-iCD45KO) into an atherosclerotic (ApoE$^{-/-}$) background (C57BL/6) and fed these mice with the western diet. Second, we tried single-cell RNA sequencing and biomedical methods to determine the molecular mechanisms behind CD45-regulation of EndoMT involved in endothelial CD45-mediated TGFβ_{1-3} and FGFR1 and its *in vivo* relevance. Our findings demonstrate that the loss of endothelial CD45 protects against EndoMT-driven atherosclerosis, promoting KLF2 expression while inhibiting TGFβ signaling and EndoMT markers.

Materials and Methods:

An expanded Materials and Methods section is available in the Supplement Materials and Methods and Supplement Table 1.

Genetic Mouse Models and Aortic Lesion Evaluation

In this study, all animal procedures were performed in compliance with institutional guidelines, and mouse protocols were approved by the Institutional Animal Care and Use Committee (IACUC) of Boston Children's Hospital, MA, USA. Both male and female mice were used. C57BL/6 mice (stock #00664), ApoE$^{-/-}$ mice (stock #002052), EC-specific Cre deleter mice (iCDH5CreERT2). Mice with tamoxifen-inducible deletion of endothelial CD45 on an ApoE$^{-/-}$ background (EC-iCD45KO/ApoE$^{-/-}$) (7 injections every other day)[36]. For controls, wild-type C57BL/6 mice bearing iCDH5 CreERT2 (denoted as WT). These mice crossed to the ApoE$^{-/-}$ (C57BL/6) background to obtain control ApoE$^{-/-}$/WT (ApoE$^{-/-}$) mice. WT and EC-iCD45KO/ApoE$^{-/-}$ were fed the western diet (WD) for 12 to 16 weeks beginning at 8 months age. We then evaluated atherosclerosis lesion size at the aortic sinus, abdominal aorta, and *face* entire aorta. The mouse heart and aorta were perfused, dissected, and subjected to quantification of atherosclerosis as previously described[37].

Cell culture

To isolate murine aortic endothelial cells (MAECs), aortas were collected and washed twice with PBS at 4 °C and then carefully stripped of fat and connective tissue. Aortas were cut into 3 mm long sections, and segments were put on the Matrigel-coated (Corning) plate with endothelial cells medium[38]. After 4 days, vascular networks were visible under the light microscope and tissue segments were removed. ECs were detached and then cultured in fresh endothelial cells medium. The identity of isolated ECs was confirmed by immunofluorescent staining using EC markers CD31. A full list of reagents including antibodies and primers is included in the supplementary information. Cultured MAECs were treated with 5 μM tamoxifen for 3 days to induce the deletion of CD45 gene from EC-iCD45KO/ApoE$^{-/-}$; iCDH5-Cre mice, MAECs

isolated from ApoE$^{-/-}$ mice as controls. Cells were treated with 100 µg/mL ox-LDL or 10ng/mL TGFβ1 at the indicated time while maintaining 2 µM tamoxifen in the medium.

Aortic sample preparation for scRNA-seq

Aortic cells were isolated as described before[36]. Mouse aortas were cut into fine pieces and placed in 5 mL of enzyme solution at 37° C. (Collected the supernatant every 10 min until all the fine pieces were digested). (Enzyme solution: 5 mL of DMEM, Collagenase type I: 5mg/mL (Gibco), Collagenase type IV:5mg/mL (Gibco), Liberase :5mg/mL (Roche). This solution was then filtered with a 40-µm strainer, centrifuged (400g for 5 minutes), and the cell pellet was suspended in 90 µL of buffer containing 0.5% BSA and 2 mmol/L EDTA in PBS. Then, 20 µL of CD31 microbeads (Miltenyi Biotec) was added to the suspension at 4° C for 15 minutes. Microbeads were passed through an LS column (Miltenyi Biotec). Cells were processed for scRNA-seq with the 10x Genomics platform, and sequencing was performed by MedGenome (Figure S1).

Data Analysis of scRNA-seq

The raw scRNA-seq data were processed using Cell Ranger (version 6.1.2) (10x Genomics). We used the Cell Ranger and R package Seurat version 4.0.2 to perform scRNA-seq analysis. In brief, we generated a normalized gene expression matrix harboring between ApoE and EC-iCD45KO/ApoE$^{-/-}$ mice. The high-quality data after these filtering steps was then used at additional processing steps including log normalization data scaling, principal component analysis (PCA), cell clustering, and UMAP visualization. Next, marker genes in each cell cluster were used to annotate cell types based on known marker genes in the database and literature. The marker gene expressions were visualized by DotPlot and VlnPlot functions. Pathway enrichment

analysis for group comparison was performed with R package ReactomeGSA. The trajectory inference for single-cell data from EndoMT models was performed with the R package Slingshot[39].

Hematoxylin and Eosin staining

Cryostat sections of mouse aortic root, abdominal aorta, and BCA were washed in PBS for 5 minutes, then fixed in 4% paraformaldehyde for 15 minutes. Next, slides were stained with hematoxylin for 3 minutes, followed by running tap water washes for 10 minutes. Slices were then dipped in eosin working solution for 30 seconds, quickly rinsed with tap water, dehydrated using graded ethanol (95% and 100% ethanol), followed by transparentizing by xylene. Slices were mounted in synthetic resin[40].

Flow cytometry analysis

Flow cytometry analysis of aortic cells from normal diet ApoE$^{-/-}$ and WD diet ApoE$^{-/-}$ (16-20 weeks) was isolated as described above. Cell pellets were resuspended in FACS buffer (2%HBSS, 0.004%FBS, 2mM EDTA in PBS) at 4°C for 30 min to block unspecific binding of antibodies to Fc receptors. Cells were incubated for antibodies for 30 min; flow cytometry analysis was performed using the BD instrument.

Oil Red O staining

Cryostat sections: cryostat sections were fixed in 4% paraformaldehyde. Slides were washed with PBS, and rinsed with 60% isopropanol, followed by staining with freshly prepared 0.5% Oil red O solution in isopropanol for 20 minutes at 37°C. Slices were then put in 60% isopropanol for 30 sec, followed by 3 washes in water, and then dried slides mounted with glycerin. Imaging

was processed with a Zeiss LSM880 microscope and analyzed with ZEN-Lite software and NIH ImageJ software.

En face Oil Red O Staining: Whole aortae were dissected symmetrically, pinned to parafilm to allow the *en face* exposed and fixed in formalin for 24hrs. The aortae were washed in PBS 3 times and rinsed in 100% propylene glycol, followed by staining with 0.5% Oil Red O solution in propylene glycol for 20 mins at 65°C. The samples were then put in 85% propylene glycol for 2 mins, followed by three washes in DD Water and then dried slides. The image was performed using a Nikon SMZ1500 stereomicroscope, SPOT Insight 2Mp Firewire digital camera, and SPOT Software 5.1.

Van Gieson's staining

Sections were fixed in 10% buffered formalin for 15 min and washed in water. Slides were stained with 3 min in Van Gieson's solution, dehydrated in 95% alcohol and 100% alcohol two times. Then, slides were cleared in xylene two times and mounted with Permount. Staining results were presented as: Collagen fibers–Red and Other tissue elements–Yellow.

RNA isolation, quantitative real-time PCR

Total RNA was extracted from primary MAECs using the RNeasy kits (Qiagen), respectively. On-column DNA digestion (Qiagen) was carried out during RNA extraction. For the synthesis of the first strand of cDNA, 1 μg of total RNA after DNase treatment was reverse transcribed using cDNA Synthesis Kit (Vazyme). Quantitative real-time PCR was performed on a CFX96 detection system (StepOnePlus Real-Time PCR Systems) with SYBR Green reagents (Vazyme). All PCR primers' sequences are presented in online supplemental table 1.

***Evaluation of EndoMT Markers by Immunostaining* In Vivo *and* In Vitro**

Samples from ApoE$^{-/-}$ and EC-iCD45KO/ ApoE$^{-/-}$ were evaluated by co-staining CD31 (or VE-cadherin) with α-SMA, KLF2, and ICAM-1. EndoMT is expressed by the overlapping percentile of CD31 (or VE-cadherin) with other markers. For *in vitro* EndoMT marker staining, mouse aortic EC (MAEC) cultures were treated with Ox-LDL (100 μg/mL) or TGFβ1 (10 ng/mL) on the indicated days.

Immunofluorescence staining

Human Tissue Paraffin Sections: Human healthy control and diseased aortic arch samples from atherosclerosis patients were purchased from Maine Medical Center Biobank (Sample ID: RA06-1040A1)[39]. The paraffin sections were de-paraffinized and performed antigen retrieval to unmask the antigenic epitope with 10 mM Sodium Citrate, pH 6.0, with 0.5% Tween 20 at 90 °C for 30 minutes. Allow the slides to cool before proceeding with staining procedure[40]. Immunofluorescence staining of the slides was performed with the standard protocol described below. Samples were blocked in PBS with donkey serum, 3% BSA, and 0.3% triton X-100 at 4°C overnight and incubated with primary antibodies VE-cadherin with CD45 at 4°C overnight[41,42]. The sections were washed three times, and respective secondary antibodies conjugated to fluorescent labels (Alexa Flour 594, 488, or 647) were added for 2 h at room temperature. The sections were mounted with Fluoroshield mounting medium containing DAPI (1:100).

Mouse aortic root and BCA cryosections: Sections were fixed by 4% paraformaldehyde for 15 min at room temperature and blocked in PBS solution containing 3% donkey and/or 10% goat serum, 3% BSA, and 0.3% Triton X-100 for 1 hour[41,42]. Samples were then incubated with primary antibody at 4°C overnight, followed by incubation with the respective secondary antibodies conjugated to fluorescent labels (Alexa Flour 594, 488, or 647; 1:200) for 2 h at room

temperature. The sections were mounted with Fluoroshield (R & D Systems) mounting medium containing DAPI (1:100).

En Face Preparation and Immunofluorescence Labeling

En face immunofluorescence was performed as described [43]. Thoracic aorta were isolated and further fixed in 2% paraformaldehyde solution at 4 °C for 1.5 hours. Fixed tissues were permeabilized in a permeabilization buffer (PBS containing 0.2% Triton X-100) for 1 hour at room temperature and subsequently incubated with a blocking buffer (5.5% FBS in permeabilization buffer) for 1 hour at room temperature. Primary antibodies were diluted in a staining buffer (2.75% FBS in permeabilization buffer) and incubated with tissue for 16 hours at 4 °C with gentle agitation. Tissues were subsequently washed 3× in the permeabilization buffer in 30-minute intervals. Secondary antibodies (conjugated with Alexa Fluor 647, Alexa Fluor 594, or Alexa Fluor 488) diluted as 1:200 working solution (10 µg/mL) in the staining buffer were added after the third wash and incubated at room temperature for 3 hours. Tissues were subsequently washed 3× in the permeabilization buffer and 1× in PBS with 30 minutes for each step. After the PBS wash, vascular tissues were bisected along the direction of flow and mounted with Fluoroshield (R & D Systems). Images were obtained using Zeiss LSM 880 with the manufacturer's software (Zen Black for microscope operation and Zen Blue for image export and analysis).

Data Analysis:

All data were analyzed by Prism 8 (GraphPad Software Inc). Data are expressed as the mean ± SEM. The means of two groups were compared using Student's t-test (unpaired, two-tailed), and one-way analysis of variance was used for comparison of more than two groups with $P < 0.05$

considered to be statistically significant. Unless otherwise indicated, all experiments were repeated at least three times.

Results:

Assess CD45 expression in atherosclerotic lesions

To confirm the localization of CD45 protein in the mouse aortic endothelial cells, we performed an immunofluorescence study on both samples in the patient atherosclerotic arch sample and mouse aortic root. We found that CD45 co-expression with VE-cadherin in the patient's aorta arch samples with severe and mild atherosclerotic lesions (Figure 1**A**); we also detected that CD45 protein expression co-expressed with CD31 in the aortic root with the atheroma of 12-week-old ApoE-null mice (Figure 1**F**). As ApoE$^{-/-}$ mice fed a normal diet also develop lesions, albeit at a slower rate compared to WD-fed ApoE$^{-/-}$ mice, we chose to use WT mice that were fed a normal chow as our true negative control for atherosclerosis occurrence to rule out the potential effect of high cholesterol content in WD-fed mice and lesion development in normal chow-fed ApoE-/- mice. (Figure 1**B**). In addition, we performed *en face* immunostaining of the thoracic aorta with antibodies to VE-Cadherin, CD31, DAPI, and CD45 (Figure 4**E**). It showed CD45 co-expression with VE-Cadherin and CD31 in wild-type ApoE-null mice but a significant reduction of CD45 expression in EC-iCD45KO ApoE-null mice. Furthermore, flow cytometry analyses of total aortic cells for VE-cadherin, FGFR1, and CD45 showed a significant reduction in VE-cadherin+/FGFR1+ ECs in WD-fed ApoE$^{-/-}$ mice, compared to normal diet-fed ApoE$^{-/-}$ mice (Figure. 1**C**, **D**). In contrast, VE-cadherin+/CD45+ ECs were greatly increased in WD-fed, ApoE-/- mice compared to normal diet-fed ApoE$^{-/-}$ mice (Figure. 1**C**), suggesting loss of FGFR1 may contribute EndoMT in lesions of WD-fed ApoE$^{-/-}$ mice.

Single-Cell RNA-Seq revealed that endothelial CD45 plays a critical role in EndoMT in an atherosclerosis mouse model

To investigate whether endothelial CD45 plays a role in EndoMT, we performed scRNA-seq analysis in the atherosclerotic ApoE$^{-/-}$ mouse model. ApoE$^{-/-}$ and EC-iCD45KO/ApoE$^{-/-}$ male mice were fed a WD for 16 weeks, followed by isolation of aortas, enzymatic digestion, and scRNA-seq (Figure S4). Overall, 2 individual samples in the compared groups yielded a similar number of cells for the subsequent analysis (cells for ApoE$^{-/-}$ and EC-iCD45KO/ApoE$^{-/-}$) after processing the data quality control underlying filtering of cells with low genes and UMIs (Figure S5), as well as dead cells as described in the Methods. We confirmed the efficacy of the CD45 knockout in aortic endothelial cells (Figure 2**B**). Using specific cell markers, we grouped EndoMT-related cell populations ECs, EndoMT (these cells express both EC and SMC markers), VSMCs, SMCs- like cells, fibroblasts, and proliferation cells. In the clusters, the ratio of ECs is higher in the EC-iCD45KO/ApoE$^{-/-}$ versus ApoE$^{-/-}$ group, whereas the ratio of EndoMT cells, VSMCs, VSMCs- like cells, and fibroblasts are higher in ApoE-/-mice (Figure 2**C**), suggesting that loss of endothelial CD45 attenuated EndoMT. The ratio of EndoMT, SMCs, SMCs-like cells, and fibroblasts cells (Figure 2**C**) confirmed the phenotype of EC-iCD45KO/ApoE$^{-/-}$ mice in atherosclerosis. Cell type–specific markers were defined relative to all other cells (Figure 2**D**). Next, we showed the expression dynamics of cell-specific markers in pseudotime. The trajectory plot in Figure 2**E**-2**J** clearly demonstrates the gene expression of representative markers specific to ECs (Pecam1) and SMCs (Acta2 and Myl9) through the EC→EndoMT→SMC process, which is shown as normalized expression. Similarly, we used the trajectory plot tested EC (Cdh5, Cldn5, Egfl7 and Tek) and SMC markers (Myh11, Tagln and Fbln5) in ApoE$^{-/-}$ and EC-iCD45KO/ApoE$^{-/-}$ aortic cells (Figure S7).

Single-Cell RNA-Seq indicated that endothelial CD45 plays a critical role in the specific EndoMT cell populations

We continue to characterize EndoMT cells into two subclusters: EndoMT1 and EndoMT2 (Figure 3**A**). This result is supported by measuring specific EC, SMC, and EndoMT markers in the EndoMT1 and EndoMT2 clusters. The violin plots in Figure 3 (**B**-**D**) show that EC markers (Cdh5, Flt1, Mecom) increased in EC-iCD45KO/ApoE$^{-/-}$ aortas compared with ApoE$^{-/-}$ aortas, but SMC markers (Mef2c, pde4d, pdcd4) and EndoMT markers (Fbln2, Fbln5, Isg15） are downregulated in EC-iCD45KO/ApoE$^{-/-}$ mice in EndoMT1 subcluster. In EndoMT2 cells, EC markers (Sparc, Bsg, Egr1) increased, but SMC markers (Ccdn3 and Foxp1) and EndoMT markers (TGFβ1, TGFβ2, Ebf1 ） decreased. Pathway analysis with genes coordinately differentially expressed in ApoE$^{-/-}$ and EC-iCD45KO/ApoE$^{-/-}$ mice (Figure 3**F**-**I**). Actin-binding pathways were decreased in EndoMT1. Endothelial cell migration, proliferation, and development pathways were enriched, while smooth muscle cell proliferation, epithelial cell development pathways were decreased in both clusters EndoMT1 and 2. Similarly, we used violin plots plot to test the other EC, EndoMT and SMC markers in EndoMT 1 and 2 clusters in ApoE$^{-/-}$ and EC-iCD45KO/ApoE$^{-/-}$ aortic cells (Figure S7).

Loss of CD45 in ECs attenuates the expression of EndoMT markers

We measured EndoMT markers in MAECs from WT and EC-iCD45KO after treating them with 100 μg/mL of oxidized low-density lipoprotein for 24 hours. It showed that endothelial CD45 knock-out attenuated the TGFβ$_{2\text{-}3}$ mRNA expression in MAECs (Figure. 4**A**). Consistently, MAECs from WT and EC-iCD45KO mice were treated with (TGFβ1 10ng/mL) for 4 days. We found that WT expressed α-SMA, but endothelial CD45 deletion leads to a reduction of α-SMA

in MAECs (Figure. 4**B**). In addition, we applied the triple-label flow cytometric method we developed for mitral valve analyses to total aortic ECs from age and gender-matched wild-type (WT) and ApoE-/- mice fed a WD for 16-20 weeks (Figure. 4**C**). (arrow) shows CD45+/VE-cadherin+/αSMA+ cells were significantly increased from 0.8 ± 1.0% in WT mice (n=3) to 9.2 ± 0.7% in ApoE-/- WD-fed mice (n=3) ($p = 0.0003$). The presence of α-SMA+ in ApoE-/- WD-fed mice indicates CD45+ ECs underwent an EndoMT in an aortic atherosclerotic lesion. Furthermore, it showed a significant upregulation of KLF2 in aortic root from EC-iCD45KO/ApoE-/- mice fed with WD 12 weeks, compared to normal CD45 wild-type ApoE-/- mice (Figure. 4**D**).

Endothelial Loss of CD45 Prevents Inflammation and Atherosclerosis

Aortic sinus, abdominal aorta, and *en face* whole aorta staining were performed to evaluate lesion ween wild-type ApoE-null and endothelial CD45 deficient WD mice. We observed a markedly reduced atherosclerotic lesion formation using aortic root (12-week WD), BCA (16-week WD), and abdominal aorta (16-week WD) in endothelial CD45 deficiency mice (Figure 5 **E-I**). Whole mount *en face* aortas from ApoE$^{-/-}$ and EC-iCD45KO/ApoE$^{-/-}$ mice were stained with Oil Red O (Figure 1**H-I**: 16-week WD; Figure 5**A-B**: 16-week WD, Figure 5**C:** 13-week WD). CD45 depletion significantly reduced atherosclerotic burden along the entire aorta in ApoE-null mice. Mice of the 2 genotypes fed with WD diet for 16 weeks showed no difference in body weights for males or females. Serum total cholesterol as well as triglycerides, HDL, LDL, levels showed no significant difference among the 2 groups of the male or female mice (data not shown). Next, we found a significant reduction of ICAM-1 expression on thoracic aorta (Figure 4**F**) and aortic root in EC-iCD45KO/ApoE$^{-/-}$ mice (Figure S3**B**). We did not detect the VCAM-1 expression has a significant difference between ApoE$^{-/-}$ and EC-iCD45KO/ApoE$^{-/-}$

mice in the aortic root (Figure S3**A**). In addition, aortic root sections from ApoE$^{-/-}$ and EC-iCD45KO/ApoE$^{-/-}$ mice (16-week WD) were co-stained with CD68 (a marker for lesion macrophages) and α-SMA. Diminished foam cell formation (Oil red o stained) and α-SMA were seen because of CD45 deficiency (Figure S2; Figure 5**D**).

Discussion

In the present study, we show for the first time that endothelial CD45 genetic deletion of the reduced atheroma burden in ApoE-null mice fed with the western diet. Our single-cell data indicated that EC-specific knock-out CD45 reduces a novel sub-population of EndoMT cells-EndMT2. We also found that CD45 deficiency led to decreased TGFβ$_{2\text{-}3}$ expression on MAECs treated with ox-LDL. In addition, we unexpectedly observed that the absence of endothelial CD45 led to the reduction of α-smooth muscle actin, which is typical of EndoMT in the aortic plaque. Finally, we found that endothelial CD45 deficiency positively correlated with KLF2 expression, which counters EndoMT.

Since CD45 is commonly used as a negative marker for ECs, the existence of CD45-positive ECs may have been overlooked in previous studies. Protein tyrosine phosphatase receptor type C (CD45)-positive endothelium has been observed in mitral valves at 6 months post-myocardial infarction and exhibited EndoMT phenotype in adult sheep[35]. Also, the CD45 phosphatase inhibitor blocked EndoMT activities in TGFβ1-treated ovine mitral valve endothelial cells [35]. We detected CD45-positive ECs on aortic arch from human patients with atherosclerosis. It indicated that endothelial CD45 plays a vital role in human atherosclerosis. The results of the present study reveal that loss of endothelial CD45 results in a favorable outcome in an animal model of

atherosclerosis. In the absence of endothelial CD45 mice on the ApoE-null background on a WD diet for 12 weeks had a 25.39% reduction in lesion size in the aortic sinus compared with ApoE-null mice expressed with CD45. On the other hand, we found that CD45-deficient ApoE-null female mice fed with the WD diet exhibited a reduction of *en face* lesion area of the entire aorta (21.82 %, 12-week WD; 36.79%, 16-week WD), compared with ApoE-null mice expressed with CD45. This notion is supported by our finding that when significant lesions (28.28≈%) were reduced at brachiocephalic artery (BCA) and a reduction of 40.05% at abdominal aorta in endothelial CD45 deficiency mice. Overall, these results clearly indicate that the lack of endothelial CD45 prevents atherosclerosis not only in the aortic sinus but also in the entire aorta.

EndoMT contributes to atherosclerotic pathobiology and is associated with more complex plaques[13]. However, the detailed molecular mechanisms underlying CD45 that drive EndoMT and the therapeutic potential of manipulating CD45 expression in atherosclerosis are entirely unknown. The single-cell RNA-seq analysis provides an unbiased overview of how the transcriptome changes in the aortic cells. Cells populated 15 major clusters after integrating the single-cell transcriptomic profiles. In the EC-iCD45KO group, the population of endothelial, resident macrophage, and mesenchymal-endothelial transition cells increased while vascular smooth muscle, EndoMT, and fibroblast cells decreased (Figure S6). In EndoMT cells, EC markers (Cdh5, Cldn5, Pecam1) increased, but SMC markers (Acta2 and Myl9), and EndoMT markers (Col1a2 and Col3a1） decreased. In addition, we characterized EndoMT cells into two sub-clusters: 1 and 2. EC-specific CD45 deletions reduced the cell numbers in the EndoMT2 sub-cluster in atherosclerotic mice but had less impact on the EndoMT1 sub-cluster. CD45 is not normally expressed in ECs, and the details of how it might regulate normal or partial EndoMT needs to be addressed. It is reported that the partial endothelial-to-mesenchymal transition is

mediated by HIF-induced CD45 upon carotid artery ligation[44]. The single-cell results of the present study identified a CD45-dependent EndoMT population in aortic endothelial cells (EndoMT2 sub-cluster), and it indicated that endothelial CD45 may mediate partial EndoMT in advanced atherosclerosis[45].

It is well established that atheroma progression is involved in inflammation during EndoMT[46]. In line with this concept, our single-cell study showed that loss of endothelial CD45 led to decreases of multiple proinflammatory cytokines in EC-iCD45KO mice, including ICAM-1(EndoMT1 sub-cluster) and CCl5 (in both EndoMT1 and EndoMT2 sub-cluster). Oxidatively modified LDL (ox-LDL) is a critical pathogenic factor in atherogenesis[47]. It demonstrated that oxidized low-density lipoprotein reduces TGFβ1 synthesis with a feedback upregulation of TGFβ1 receptors and concurrently increases the expression of ICAM-1 in human coronary artery endothelial cells[48]. Consistently, we observed a reduction of ICAM-1 expression in mouse thoracic aorta and aortic sinus in the EC-iCD45KO/ApoE$^{-/-}$ mice. These data are associated and consistent with the reduced atherosclerosis results. Strikingly, the endothelial CD45-specific endothelial knockout ablate TGFβ signaling genetically confined to the MAECs, reduced ox-LDL-induced gene expression, including TGFβ$_{2-3}$. Our flow cytometry data from ECs highlight a significant reduction of FGFR1- ECs in ApoE$^{-/-}$ WD aortas which indicates ECs undergo EndoMT in atherosclerosis since FGFR1 inhibits TGFβ during EndoMT[49]. In contrast, a marked increase in the expression of KLF2 in CD45 EC-iCD45KO/ApoE$^{-/-}$ at the aortic root. Unlike KLF4, KLF2 is not directly regulated by TGFβ signaling. Nevertheless, KLF2 appear functionally important given a known interaction among other KLFs. TGFβR2 disruption, may lead to a small rise in KLF4 levels and thereby increasing KLF2[50-52].

In summary, we report the first evidence that in ApoE-null mice fed with WD, the absence of endothelial CD45 leads to reduced lesion development, foam cells, plaque macrophages, and expression of adhesion molecules, which is negatively associated with the degree of atherosclerosis. In addition, endothelial CD45 deficiency led to a downregulation of the expression of TGF$\beta_{2\text{-}3}$, cytokines CCl5, and α-SMA while an upregulation of KLF2 expression; coincides with CD45-deficiency-mediated reduction of EndoMT and inflammation in atherosclerosis. These findings highlight the novel function of CD45 in endothelial cells in relation to EndoMT-driven atherosclerosis, the leading cause of death in the United States.

References

1. Martin SS, Aday AW, Almarzooq ZI, et al. 2024 Heart Disease and Stroke Statistics: A Report of US and Global Data From the American Heart Association. *Circulation.* Feb 20 2024;149(8):e347-e913.
2. Sorokin V, Vickneson K, Kofidis T, et al. Role of Vascular Smooth Muscle Cell Plasticity and Interactions in Vessel Wall Inflammation. *Front Immunol.* 2020;11:599415.
3. Khatana C, Saini NK, Chakrabarti S, et al. Mechanistic Insights into the Oxidized Low-Density Lipoprotein-Induced Atherosclerosis. *Oxid Med Cell Longev.* 2020;2020:5245308.
4. Lorey MB, Oorni K, Kovanen PT. Modified Lipoproteins Induce Arterial Wall Inflammation During Atherogenesis. *Front Cardiovasc Med.* 2022;9:841545.
5. Gencer S, Evans BR, van der Vorst EPC, Doring Y, Weber C. Inflammatory Chemokines in Atherosclerosis. *Cells.* Jan 25 2021;10(2).
6. Farahi L, Sinha SK, Lusis AJ. Roles of Macrophages in Atherogenesis. *Front Pharmacol.* 2021;12:785220.
7. Gialeli C, Shami A, Goncalves I. Extracellular matrix: paving the way to the newest trends in atherosclerosis. *Curr Opin Lipidol.* Oct 1 2021;32(5):277-285.
8. Moore KJ, Tabas I. Macrophages in the pathogenesis of atherosclerosis. *Cell.* Apr 29 2011;145(3):341-355.
9. Jebari-Benslaiman S, Galicia-Garcia U, Larrea-Sebal A, et al. Pathophysiology of Atherosclerosis. *Int J Mol Sci.* Mar 20 2022;23(6).
10. Gimbrone MA, Jr., Garcia-Cardena G. Endothelial Cell Dysfunction and the Pathobiology of Atherosclerosis. *Circ Res.* Feb 19 2016;118(4):620-636.
11. Kovacic JC, Dimmeler S, Harvey RP, et al. Endothelial to Mesenchymal Transition in Cardiovascular Disease: JACC State-of-the-Art Review. *J Am Coll Cardiol.* Jan 22 2019;73(2):190-209.
12. Kovacic JC, Mercader N, Torres M, Boehm M, Fuster V. Epithelial-to-mesenchymal and endothelial-to-mesenchymal transition: from cardiovascular development to disease. *Circulation.* Apr 10 2012;125(14):1795-1808.
13. Evrard SM, Lecce L, Michelis KC, et al. Endothelial to mesenchymal transition is common in atherosclerotic lesions and is associated with plaque instability. *Nat Commun.* Jun 24 2016;7:11853.
14. Chen PY, Qin L, Baeyens N, et al. Endothelial-to-mesenchymal transition drives atherosclerosis progression. *J Clin Invest.* Oct 26 2015;125(12):4514-4528.
15. Lertkiatmongkol P, Liao D, Mei H, Hu Y, Newman PJ. Endothelial functions of platelet/endothelial cell adhesion molecule-1 (CD31). *Curr Opin Hematol.* May 2016;23(3):253-259.
16. Breviario F, Caveda L, Corada M, et al. Functional properties of human vascular endothelial cadherin (7B4/cadherin-5), an endothelium-specific cadherin. *Arterioscler Thromb Vasc Biol.* Aug 1995;15(8):1229-1239.
17. Peng Q, Shan D, Cui K, et al. The Role of Endothelial-to-Mesenchymal Transition in Cardiovascular Disease. *Cells.* Jun 3 2022;11(11).
18. Korhonen EA, Lampinen A, Giri H, et al. Tie1 controls angiopoietin function in vascular remodeling and inflammation. *J Clin Invest.* Sep 1 2016;126(9):3495-3510.
19. Piera-Velazquez S, Jimenez SA. Endothelial to Mesenchymal Transition: Role in Physiology and in the Pathogenesis of Human Diseases. *Physiol Rev.* Apr 1 2019;99(2):1281-1324.
20. Piera-Velazquez S, Li Z, Jimenez SA. Role of endothelial-mesenchymal transition (EndoMT) in the pathogenesis of fibrotic disorders. *Am J Pathol.* Sep 2011;179(3):1074-1080.

21. Ursoli Ferreira F, Eduardo Botelho Souza L, Hassibe Thome C, et al. Endothelial Cells Tissue-Specific Origins Affects Their Responsiveness to TGF-beta2 during Endothelial-to-Mesenchymal Transition. *Int J Mol Sci.* Jan 22 2019;20(3).

22. Chen PY, Qin L, Li G, et al. Endothelial TGF-beta signalling drives vascular inflammation and atherosclerosis. *Nat Metab.* Sep 2019;1(9):912-926.

23. Gross MD, Bielinski SJ, Suarez-Lopez JR, et al. Circulating soluble intercellular adhesion molecule 1 and subclinical atherosclerosis: the Coronary Artery Risk Development in Young Adults Study. *Clin Chem.* Feb 2012;58(2):411-420.

24. Pickett JR, Wu Y, Zacchi LF, Ta HT. Targeting endothelial vascular cell adhesion molecule-1 in atherosclerosis: drug discovery and development of vascular cell adhesion molecule-1-directed novel therapeutics. *Cardiovasc Res.* Oct 24 2023;119(13):2278-2293.

25. Luo W, Liu A, Chen Y, et al. Inhibition of accelerated graft arteriosclerosis by gene transfer of soluble fibroblast growth factor receptor-1 in rat aortic transplants. *Arterioscler Thromb Vasc Biol.* Jun 2004;24(6):1081-1086.

26. Yang X, Liaw L, Prudovsky I, et al. Fibroblast growth factor signaling in the vasculature. *Curr Atheroscler Rep.* Jun 2015;17(6):509.

27. Chen PY, Simons M. Fibroblast growth factor-transforming growth factor beta dialogues, endothelial cell to mesenchymal transition, and atherosclerosis. *Curr Opin Lipidol.* Oct 2018;29(5):397-403.

28. Chen PY, Qin L, Barnes C, et al. FGF regulates TGF-beta signaling and endothelial-to-mesenchymal transition via control of let-7 miRNA expression. *Cell Rep.* Dec 27 2012;2(6):1684-1696.

29. Ma J, Sanchez-Duffhues G, Goumans MJ, Ten Dijke P. TGF-beta-Induced Endothelial to Mesenchymal Transition in Disease and Tissue Engineering. *Front Cell Dev Biol.* 2020;8:260.

30. Lingrel JB, Pilcher-Roberts R, Basford JE, et al. Myeloid-specific Kruppel-like factor 2 inactivation increases macrophage and neutrophil adhesion and promotes atherosclerosis. *Circ Res.* May 11 2012;110(10):1294-1302.

31. Justement LB. The Role of CD45 in Signal Transduction. In: Dixon FJ, ed. *Advances in Immunology.* Vol 66: Academic Press; 1997:1-65.

32. Forsyth KD, Chua KY, Talbot V, Thomas WR. Expression of the leukocyte common antigen CD45 by endothelium. *The Journal of Immunology.* 1993;150(8):3471-3477.

33. Hong J, Wong B, Huynh C, et al. Tm4sf1-marked Endothelial Subpopulation Is Dysregulated in Pulmonary Arterial Hypertension. *Am J Respir Cell Mol Biol.* Apr 2023;68(4):381-394.

34. Nasim S, Wylie-Sears J, Gao X, et al. CD45 Is Sufficient to Initiate Endothelial-to-Mesenchymal Transition in Human Endothelial Cells-Brief Report. *Arterioscler Thromb Vasc Biol.* May 2023;43(5):e124-e131.

35. Bischoff J, Casanovas G, Wylie-Sears J, et al. CD45 Expression in Mitral Valve Endothelial Cells After Myocardial Infarction. *Circ Res.* Nov 11 2016;119(11):1215-1225.

36. Dong Y, Wang B, Du M, et al. Targeting Epsins to Inhibit Fibroblast Growth Factor Signaling While Potentiating Transforming Growth Factor-beta Signaling Constrains Endothelial-to-Mesenchymal Transition in Atherosclerosis. *Circulation.* Feb 21 2023;147(8):669-685.

37. Dong Y, Lee Y, Cui K, et al. Epsin-mediated degradation of IP3R1 fuels atherosclerosis. *Nat Commun.* Aug 7 2020;11(1):3984.

38. Wang J-M, Chen AF, Zhang K. Isolation and Primary Culture of Mouse Aortic Endothelial Cells. *JoVE.* 2016/12/19 2016(118):e52965.

39. Cui K, Gao X, Wang B, et al. Epsin Nanotherapy Regulates Cholesterol Transport to Fortify Atheroma Regression. *Circ Res.* Jan 6 2023;132(1):e22-e42.

40. Zhu B, Gupta K, Cui K, et al. Targeting Liver Epsins Ameliorates Dyslipidemia in Atherosclerosis. *bioRxiv.* 2024.

41. Lin Y, Li LL, Nie W, et al. Brain activity regulates loose coupling between mitochondrial and cytosolic Ca(2+) transients. *Nat Commun.* Nov 21 2019;10(1):5277.

42. Pan H, Xue C, Auerbach BJ, et al. Single-Cell Genomics Reveals a Novel Cell State During Smooth Muscle Cell Phenotypic Switching and Potential Therapeutic Targets for Atherosclerosis in Mouse and Human. *Circulation.* Nov 24 2020;142(21):2060-2075.

43. Lu YW, Martino N, Gerlach BD, et al. MEF2 (Myocyte Enhancer Factor 2) Is Essential for Endothelial Homeostasis and the Atheroprotective Gene Expression Program. *Arterioscler Thromb Vasc Biol.* Mar 2021;41(3):1105-1123.

44. Yamashiro Y, Ramirez K, Nagayama K, et al. Partial endothelial-to-mesenchymal transition mediated by HIF-induced CD45 in neointima formation upon carotid artery ligation. *Cardiovasc Res.* Jul 4 2023;119(7):1606-1618.

45. Alvandi Z, Bischoff J. Endothelial-Mesenchymal Transition in Cardiovascular Disease. *Arterioscler Thromb Vasc Biol.* Sep 2021;41(9):2357-2369.

46. Chen PY, Schwartz MA, Simons M. Endothelial-to-Mesenchymal Transition, Vascular Inflammation, and Atherosclerosis. *Front Cardiovasc Med.* 2020;7:53.

47. Steinberg D. The LDL modification hypothesis of atherogenesis: an update. *J Lipid Res.* Apr 2009;50 Suppl(Suppl):S376-381.

48. Chen H, Li D, Saldeen T, Mehta JL. Transforming growth factor-beta(1) modulates oxidatively modified LDL-induced expression of adhesion molecules: role of LOX-1. *Circ Res.* Dec 7 2001;89(12):1155-1160.

49. Goumans MJ, Ten Dijke P. TGF-beta Signaling in Control of Cardiovascular Function. *Cold Spring Harb Perspect Biol.* Feb 1 2018;10(2).

50. Chen PY, Qin L, Li G, et al. Smooth Muscle Cell Reprogramming in Aortic Aneurysms. *Cell Stem Cell.* Apr 2 2020;26(4):542-557 e511.

51. Chen PY, Qin L, Simons M. TGFbeta signaling pathways in human health and disease. *Front Mol Biosci.* 2023;10:1113061.

52. Boon RA, Fledderus JO, Volger OL, et al. KLF2 suppresses TGF-beta signaling in endothelium through induction of Smad7 and inhibition of AP-1. *Arterioscler Thromb Vasc Biol.* Mar 2007;27(3):532-539.

Figure Legends

Figure 1. Endothelial CD45 dependent EndoMT during atherosclerosis. Immunostaining of aortic arch section from atherosclerosis patients with VE-cadherin (endothelial junctions, red), and CD45 protein(green) (**A**), and aortic root with CD31(red) and CD45 protein(green) from ApoE$^{-/-}$ and EC-iCD45KO/ApoE$^{-/-}$ mice fed with western diet (WD) for 12 weeks (**F**). **B**, Aortas from ApoE$^{-/-}$ mice fed a normal diet versus WD, —lesions are apparent in ApoE$^{-/-}$ WD-fed aortas. **C**, Representative flow cytometry data from ECs labeled with anti-VE-cadherin-FITC, anti-CD45-CF647, and anti-FGFR1-PE. Circles highlight increased FGFR1-ECs in ApoE$^{-/-}$ WD aortas. Squares indicate increased CD45 ECs in WD-fed aortas from ApoE$^{-/-}$ mice. **D**, Cytometric analysis from ApoE$^{-/-}$ normal diet (circles, n=3) and ApoE$^{-/-}$ WD (squares, n=5) mice. FGFR1+ECs are decreased (p=0.0324) in ApoE$^{-/-}$ WD-fed mice aortas. **E**, Diagram showing the timeline for the deletion induction by tamoxifen injections and atherosclerotic progression. **G**, Aortas from ApoE$^{-/-}$ mice versus EC-iCD45KO/ApoE$^{-/-}$ mice fed with western diet (WD) for 16 weeks (—lesions are apparent in ApoE-/-WD-fed aortas). **H**, *En face* aortas from ApoE$^{-/-}$ and EC-iCD45KO / ApoE$^{-/-}$ female mice stained with Oil Red O (16-week WD). **I**, Statistics for *En face* ORO staining (**A**: Scale bars = 10 μM), **F**: Scale bars = 5 μM).

Figure 2. scRNA-seq analysis reveals that endothelial CD45 mediated EndoMT during atherosclerosis. **A**, Cell type clusters of ApoE$^{-/-}$ and EC-iCD45KO/ApoE$^{-/-}$ mice, including endothelial cells (ECs), endothelial-to-mesenchymal transition (EndoMT) cells, vascular smooth muscle cells (VSMCs), fibroblasts, VSMC-like cells, and proliferation cell types. **B**, Expression level of CD45 (*PTPRC*) among the different cell populations. **C**, Proportion of ECs, EndoMT, VSMCs, fibroblasts, VSMC-like cells, and proliferation cells. **D**, Dot plot of selected marker genes for each cell cluster. Dot size indicates the percentage of cells expressing each gene, and dot color

indicates the expression level. **E-J**, Gene expression of representative markers specific to ECs (*Pecam1*) and SMCs (*Acta2 and Myl9*) through the EC→EndoMT→SMC process is shown as normalized expression vs UMAP_1 (also refer to Figure S7 for more marker genes).

Figure 3. **scRNA-seq analysis differential CD45-driven EndoMT on distinct cell populations.** **A**, Cell type clusters of ApoE$^{-/-}$ (6476 cells) and EC-ICD45KO/ApoE$^{-/-}$ (7021 cells) mice, including endothelial cells (ECs), endothelial-to-mesenchymal transition (EndoMT) cells, and smooth muscle cells (SMCs). EndoMT clusters were further divided into 2 subgroups: EndoMT1 and EndoMT2. Violin plots of EC (**B**), SMC (**C**), and EndoMT(**D**) markers differentially expressed in ApoE-/- and EC-ICD45KO/ApoE$^{-/-}$ mice. In the EndoMT1 subgroups of EC marker–positive cells (*Cdh5*, Flt1, Mecom), SMC marker–positive cells (Mef2c, Pde4d, Pdcd4) and EndoMT marker-positive cells (Fbln2, Fbln5, Lsg15) were analyzed. In the EndoMT2 subgroups of EC marker–positive cells (*Sparc, Bsg, Egr1*), SMC marker–positive cells (Ccnd3, Foxop1) and EndoMT marker- positive cells (TGFβ1, TGFβ2, Ebf1) were analyzed. Pathway analysis with genes coordinately differentially expressed in ApoE-/- and EC-ICD45KO/ApoE− mice (**F-I**).

Figure 4. Endothelial CD45- deficiency inhibits EndoMT by reducing TGFβ signaling and upregulates KLF2 expression during atherosclerosis. A, Mouse aortic endothelial cells (MAECs) of wild-type (WT/ApoE$^{-/-}$) and EC-iCD45KO were treated with 5 μmol/L tamoxifen for 3 days, followed by treatment with 100 μg/mL oxidized low-density lipoprotein, and then collected cell lysis for quantitative polymerase chain reaction to detect endothelial-to-mesenchymal transition (EndoMT) markers TGFβ2 and TGFβ3(n=3). **B**, IF staining to detect CD31 and α-SMA. Similarly, MAECs of wild-type and EC-iCD45KO were isolated and were treated with 5 μmol/L tamoxifen for 3 days, followed by treatment with 10 ng/mL transforming growth factor-β (TGFβ1) for 4 days, with a change to fresh medium and TGFβ1 every other day. **C**, Aortic ECs from WT

and ApoE$^{-/-}$ mice fed a western diet (WD) were labeled with fluorescently-conjugated antibodies to VE-cadherin, CD45, and α-SMA and then analyzed by flow cytometry. The red arrow indicates significantly more triple-positive cells in ApoE$^{-/-}$WD mice, which is suggestive of a CD45^{+} EndoMT during atherosclerosis. **D**, IF staining for KLF-2 (green), VE-cadherin (red), and DAPI (blue) on the luminal surface of mouse aortic root sections. (Scale bars = 5 μM). **E**, *En face* immunostaining of the thoracic aorta was performed with antibodies to VE-Cadherin, CD31, DAPI (nuclei), and either (**E**) CD45 or (**F**) ICAM-1 (**B**, **D** Scale bars = 5 μM; **E**, Scale bars = 50 μM; **F**: Scale bars = 10 μM).

Figure 5. Endothelial CD45 deletion reduces atherosclerosis in the ApoE$^{-/-}$ mouse model. A, *En face* aortas from ApoE$^{-/-}$ and EC-iCD45KO /ApoE$^{-/-}$ female (**B**, 12-week WD) and male mice (**C**, 13-week WD) stained with Oil Red O. **B**, Statistics for *en face* oil red o staining in female mice. **D**, aortic root sections from ApoE$^{-/-}$ and EC-iCD45KO ApoE$^{-/-}$ mice were stained with the macrophage marker CD68 and α-SMA. Hematoxylin and Eosin (**H&E**) staining for aortic root (**E**); aortic aneurysm sections (**G**); and brachiocephalic artery (**I**). Statistics for **H&E** staining in the aortic root (**F**), aortic aneurysm sections (**H**), and brachiocephalic artery (**J**). (Scale bars = 20 μM).

Figure S1. **Overview of animal models**. （**A**） and (**B**), workflow of generation of CD45.1 fl/fl , CD45.2 $^{-/-}$ (EC-iCD45KO) /ApoE$^{-/-}$mouse , ApoE $^{-/-}$ as control group.

Figure S2. **Loss of endothelial CD45 reduces atherosclerosis in ApoE$^{-/-}$ atherosclerotic mice.**

Aortic root (**A**), and aortic aneurysm sections(**C**) from WT and EC-iCD45KO mice (16 week-WD) stained with Oil Red O. Statistics for *En face* ORO staining in aortic root (**B**) and aortic aneurysm sections (**D**). **E**, Brachiocephalic artery (BCA) sections from ApoE-/- or EC-iCD45KO

ApoE-/- mice were stained with the macrophage marker CD68 and α-SMA. **F**, Van Gieson's stain gives collagen a pink color (arrows) and other tissue elements a yellow color in mouse aortic BCA (Scale bars = 20 μM).

S3. **Loss of endothelial CD45 reduces inflammation in ApoE−/− atherosclerotic mice. A,** VCAM-1 (Vascular cell adhesion molecule 1 red), CD31(green), and DAPI (blue) on the luminal surface of aortic root sections (12-week WD). **B**, ICAM-1 (intercellular adhesion molecule-1, red) CD31 (green), and DAPI (blue) on the luminal surface of aortic root sections (16-week WD).

Figure S4. Steps for preparation of aortic cells scRNA-seq data. WT and EC-iCD45KO male mice were fed a western diet for 16 weeks, followed by the isolation of aortas, enzyme digestion, CD31 beads enrichment endothelial cells, and single cell suspension were prepared by manufacturer's instructions. 10X Genomics- Single-cell cDNA library preparation: barcoding cells for 10 x genomics, cDNA library construction and sc-RNA sequencing. cDNA library sequencing and computational analysis: Then the sequencing reads were preprocessed by cell ranger, and downstream analysis was done.

S5. Data quality control (QC) for sc-RNA sequencing. Data quality control (QC) for sc-RNA sequencing: ApoE$^{-/-}$:21745 genes from 11497 cells; EC-iCD45KO/ApoE$^{-/-}$: 21436 genes from 16273 cells.

S6. Cell type clusters of ApoE$^{-/-}$and EC-iCD45KO/ApoE$^{-/-}$ mice.

A, Cell type clusters of ApoE$^{-/-}$ and EC-iCD45KO/ApoE$^{-/-}$ mice, including endothelial cells (ECs), endothelial-to-mesenchymal transition (EndoMT) cells, vascular smooth muscle cells (VSMCs), fibroblasts, VSMC-like cells, proliferation cells, mesenchymal-like cells, MEndoT cells, B cells, T cells, Schwann cells, Trem2 macrophages, inflammatory macrophages, resident – like

macrophages, monocytes and monocytes derived dendritic cells. **B**, Proportion of endothelial cells (ECs), endothelial-to-mesenchymal transition (EndoMT) cells, vascular smooth muscle cells (VSMCs), fibroblasts, VSMC-like cells, proliferation cells, mesenchymal-like cells, MEndoT cells, B cells, T cells, Schwann cells, Trem2 macrophages, inflammatory macrophages, resident – like macrophages, monocytes and monocytes derived dendritic cells.

S7. scRNA-seq analysis for ECs and SMCs markers in ApoE$^{-/-}$ and EC-iCD45KO/ApoE$^{-/-}$ mouse. **A**, RNA velocity analysis showed EndoMT transition down-regulated in EC-iCD45KO/ApoE$^{-/-}$ mouse. **B**, CDH5 is up-regulated in MEndoT cells of EC-iCD45KO/ApoE$^{-/-}$ that indicates Mesenchymal to EC transition in endothelial specific knock-out mice. **C**, Gene expression of representative markers specific to ECs (Cldn5, Egfl7, Cdh5) and SMCs (Myh11, Tagln, Fbln5) through the EC→EndoMT→SMC process is shown as normalized expression vs UMAP_1.

S8. scRNA-seq analysis for ECs and SMCs markers on EndMT1 and EndMT2 subcluster between ApoE$^{-/-}$ and EC-iCD45KO/ApoE$^{-/-}$ mouse. **A**, Trajectory analysis for ApoE$^{-/-}$ and EC-iCD45KO/ApoE$^{-/-}$ in mouse aortic cells (ECs as root). **B**, Proportion of ECs, EndoMT1, EndoMT2, VSMCs, fibroblasts, VSMC-like cells, and proliferation cells. **C-D**, Gene expression of representative markers specific to ECs (Cdh5) and SMCs (*Acta2, Col1a2, Sparc, Ly6a, and Pde4d*) through the EC→EndoMT→SMC process is shown as normalized expression vs UMAP_1. Violin plots of EC (**E**), SMC (**F**), and EndoMT (**G**) markers differentially expressed in ApoE-/- and EC-iCD45KO/ApoE-/- mice. In the EndoMT1 subgroups of EC marker–positive cells (Ly6a, Emcn, Sem6a), SMC marker–positive cells (Foxp1, Col8a1, Itga4) and EndoMT marker-positive cells (Ebf1, Bgn) were analyzed. In the EndoMT2 subgroups of EC marker–positive cells (Calr, Nf1,

Nr2f2), SMC marker–positive cells (Silk) and EndoMT marker-positive cells (Ets1, Btg1) were analyzed.

Figure 1

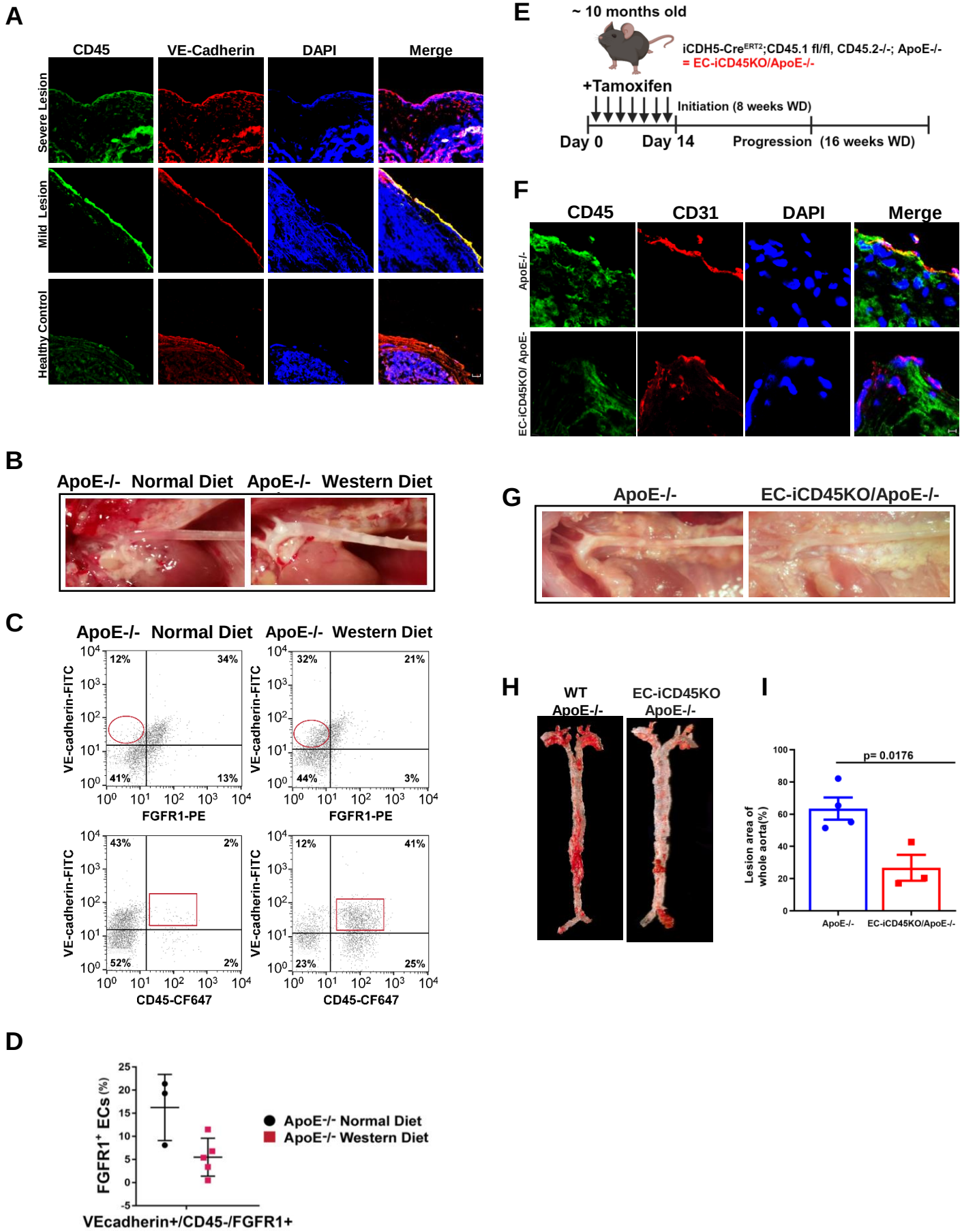
A
CD45
VE-Cadherin
DAPI
Merge
Severe Lesion
Mild Lesion
Healthy Control
B
ApoE-/- Normal Diet
ApoE-/- Western Diet
C
ApoE-/- Normal Diet
ApoE-/- Western Diet
VE-cadherin-FITC
FGFR1-PE
CD45-CF647
12%
34%
41%
13%
32%
21%
44%
3%
43%
2%
52%
2%
12%
41%
23%
25%
D
FGFR1+ ECs (%)
ApoE-/- Normal Diet
ApoE-/- Western Diet
VEcadherin+/CD45-/FGFR1+
E
~ 10 months old
iCDH5-CreERT2;CD45.1 fl/fl, CD45.2-/-; ApoE-/-
= EC-iCD45KO/ApoE-/-
+Tamoxifen
Initiation (8 weeks WD)
Day 0
Day 14
Progression (16 weeks WD)
F
CD45
CD31
DAPI
Merge
ApoE-/-
EC-iCD45KO/ ApoE-
G
ApoE-/-
EC-iCD45KO/ApoE-/-
H
WT
ApoE-/-
EC-iCD45KO
ApoE-/-
I
p= 0.0176
Lesion area of whole aorta(%)
ApoE-/-
EC-iCD45KO/ApoE-/-

Figure 2

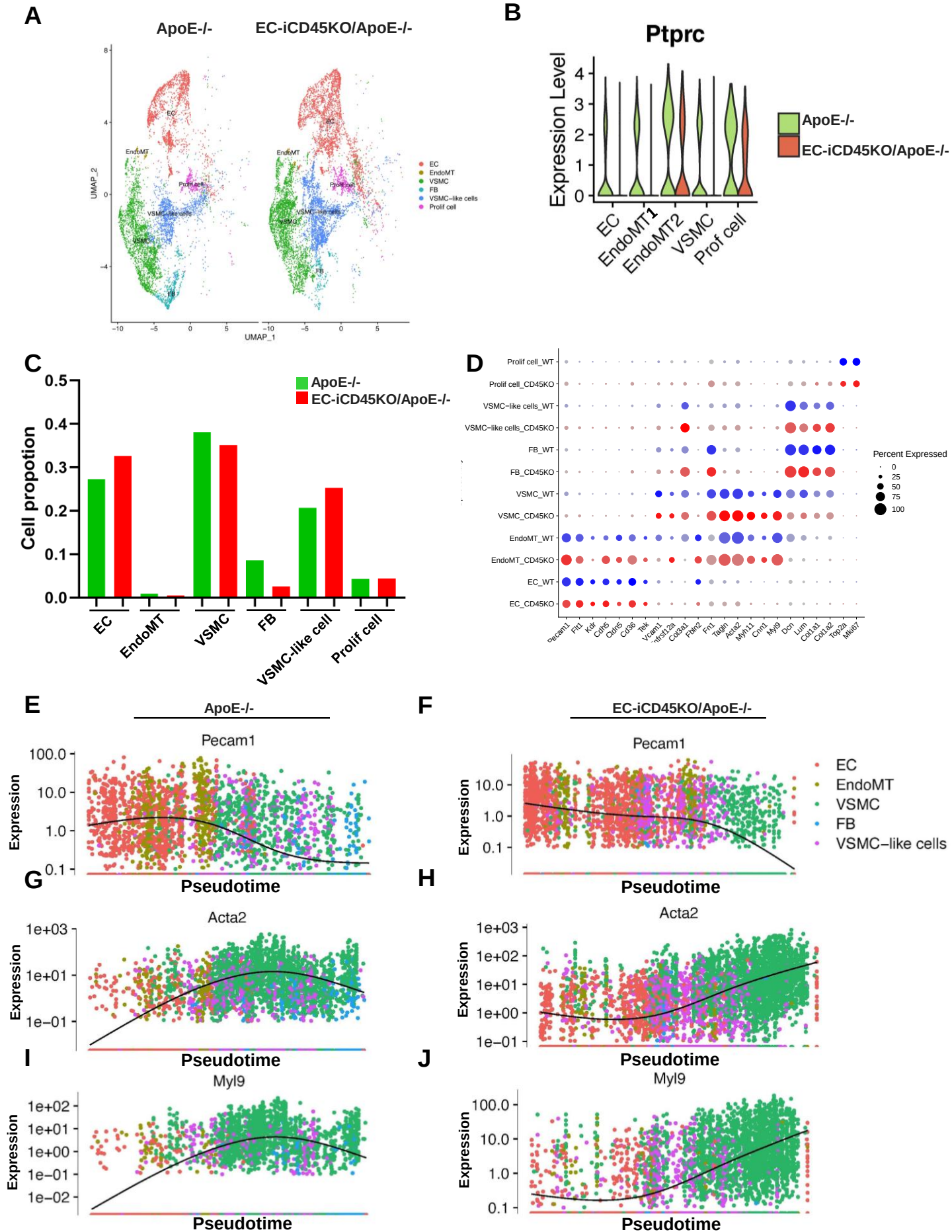
A
ApoE-/-
EC-iCD45KO/ApoE-/-
UMAP_2
UMAP_1
EC
EndoMT
VSMC
FB
VSMC−like cells
Prolif cell
B
Ptprc
Expression Level
ApoE-/-
EC-iCD45KO/ApoE-/-
EC
EndoMT1
EndoMT2
VSMC
Prof cell
C
Cell propotion
ApoE-/-
EC-iCD45KO/ApoE-/-
EC
EndoMT
VSMC
FB
VSMC-like cell
Prolif cell
D
Prolif cell_WT
Prolif cell_CD45KO
VSMC−like cells_WT
VSMC−like cells_CD45KO
FB_WT
FB_CD45KO
VSMC_WT
VSMC_CD45KO
EndoMT_WT
EndoMT_CD45KO
EC_WT
EC_CD45KO
Percent Expressed
Pecam1
Flt1
Kdr
Cdh5
Cldn5
Cd36
Tek
Vcam1
Col3a1
Fbln2
Fn1
Tagln
Acta2
Myh11
Cnn1
Myl9
Dcn
Lum
Col1a1
Col1a2
Top2a
Mki67
E
ApoE-/-
Pecam1
Expression
Pseudotime
F
EC-iCD45KO/ApoE-/-
Pecam1
Expression
Pseudotime
EC
EndoMT
VSMC
FB
VSMC−like cells
G
Acta2
Expression
Pseudotime
H
Acta2
Expression
Pseudotime
I
Myl9
Expression
Pseudotime
J
Myl9
Expression
Pseudotime

Figure 3

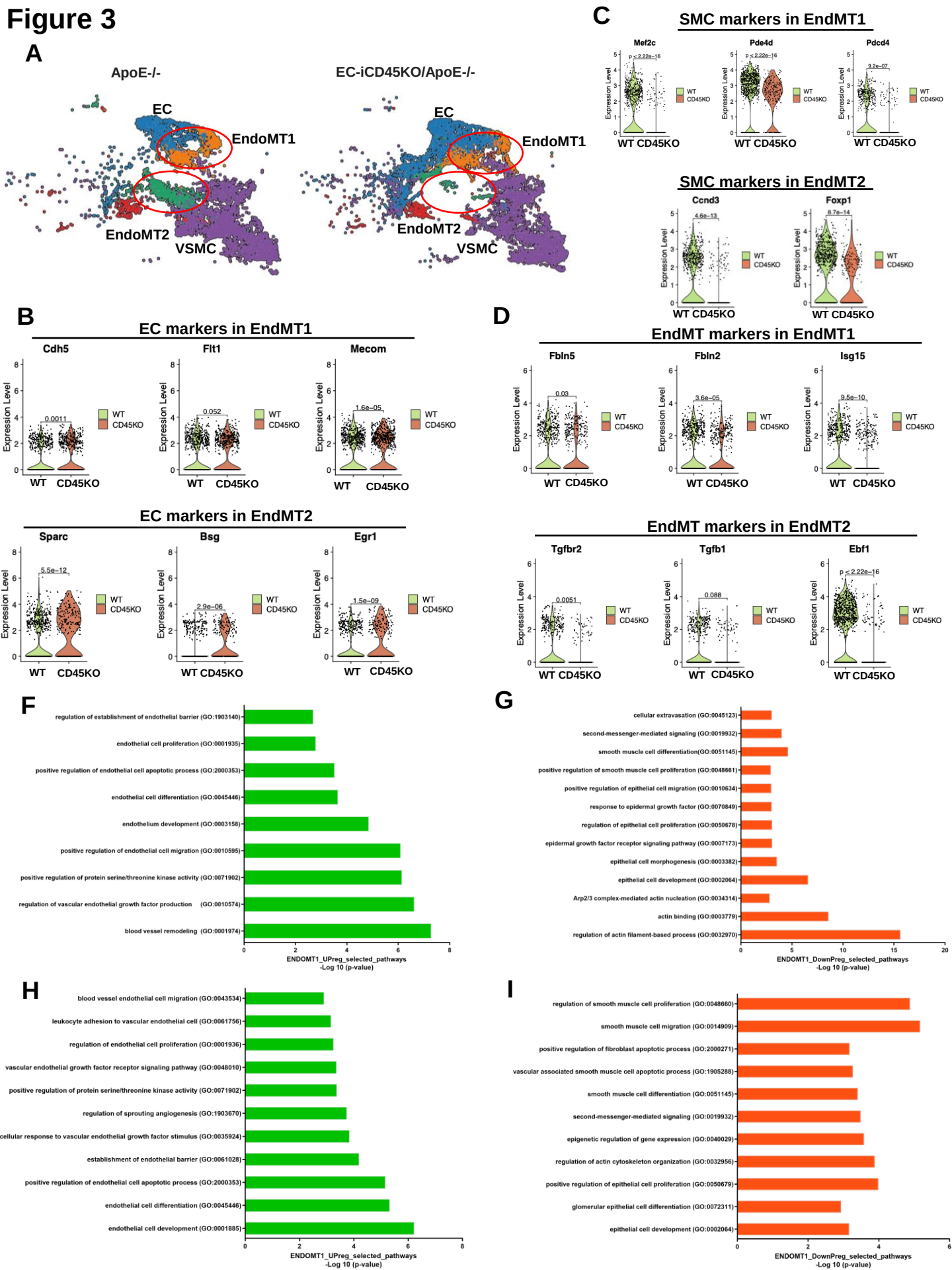
A
ApoE-/-
EC-iCD45KO/ApoE-/-
EC
EndoMT1
EndoMT2
VSMC
B
EC markers in EndMT1
Cdh5
Flt1
Mecom
EC markers in EndMT2
Sparc
Bsg
Egr1
C
SMC markers in EndMT1
Mef2c
Pde4d
Pdcd4
SMC markers in EndMT2
Ccnd3
Foxp1
D
EndMT markers in EndMT1
Fbln5
Fbln2
Isg15
EndMT markers in EndMT2
Tgfbr2
Tgfb1
Ebf1
Expression Level
WT
CD45KO
F
regulation of establishment of endothelial barrier (GO:1903140)
endothelial cell proliferation (GO:0001935)
positive regulation of endothelial cell apoptotic process (GO:2000353)
endothelial cell differentiation (GO:0045446)
endothelium development (GO:0003158)
positive regulation of endothelial cell migration (GO:0010595)
positive regulation of protein serine/threonine kinase activity (GO:0071902)
regulation of vascular endothelial growth factor production (GO:0010574)
blood vessel remodeling (GO:0001974)
ENDOMT1_UPreg_selected_pathways
-Log 10 (p-value)
G
cellular extravasation (GO:0045123)
second-messenger-mediated signaling (GO:0019932)
smooth muscle cell differentiation(GO:0051145)
positive regulation of smooth muscle cell proliferation (GO:0048661)
positive regulation of epithelial cell migration (GO:0010634)
response to epidermal growth factor (GO:0070849)
regulation of epithelial cell proliferation (GO:0050678)
epidermal growth factor receptor signaling pathway (GO:0007173)
epithelial cell morphogenesis (GO:0003382)
epithelial cell development (GO:0002064)
Arp2/3 complex-mediated actin nucleation (GO:0034314)
actin binding (GO:0003779)
regulation of actin filament-based process (GO:0032970)
ENDOMT1_DownPreg_selected_pathways
-Log 10 (p-value)
H
blood vessel endothelial cell migration (GO:0043534)
leukocyte adhesion to vascular endothelial cell (GO:0061756)
regulation of endothelial cell proliferation (GO:0001936)
vascular endothelial growth factor receptor signaling pathway (GO:0048010)
positive regulation of protein serine/threonine kinase activity (GO:0071902)
regulation of sprouting angiogenesis (GO:1903670)
cellular response to vascular endothelial growth factor stimulus (GO:0035924)
establishment of endothelial barrier (GO:0061028)
positive regulation of endothelial cell apoptotic process (GO:2000353)
endothelial cell differentiation (GO:0045446)
endothelial cell development (GO:0001885)
ENDOMT1_UPreg_selected_pathways
-Log 10 (p-value)
I
regulation of smooth muscle cell proliferation (GO:0048660)
smooth muscle cell migration (GO:0014909)
positive regulation of fibroblast apoptotic process (GO:2000271)
vascular associated smooth muscle cell apoptotic process (GO:1905288)
smooth muscle cell differentiation (GO:0051145)
second-messenger-mediated signaling (GO:0019932)
epigenetic regulation of gene expression (GO:0040029)
regulation of actin cytoskeleton organization (GO:0032956)
positive regulation of epithelial cell proliferation (GO:0050679)
glomerular epithelial cell differentiation (GO:0072311)
epithelial cell development (GO:0002064)
ENDOMT1_DownPreg_selected_pathways
-Log 10 (p-value)

Figure 4

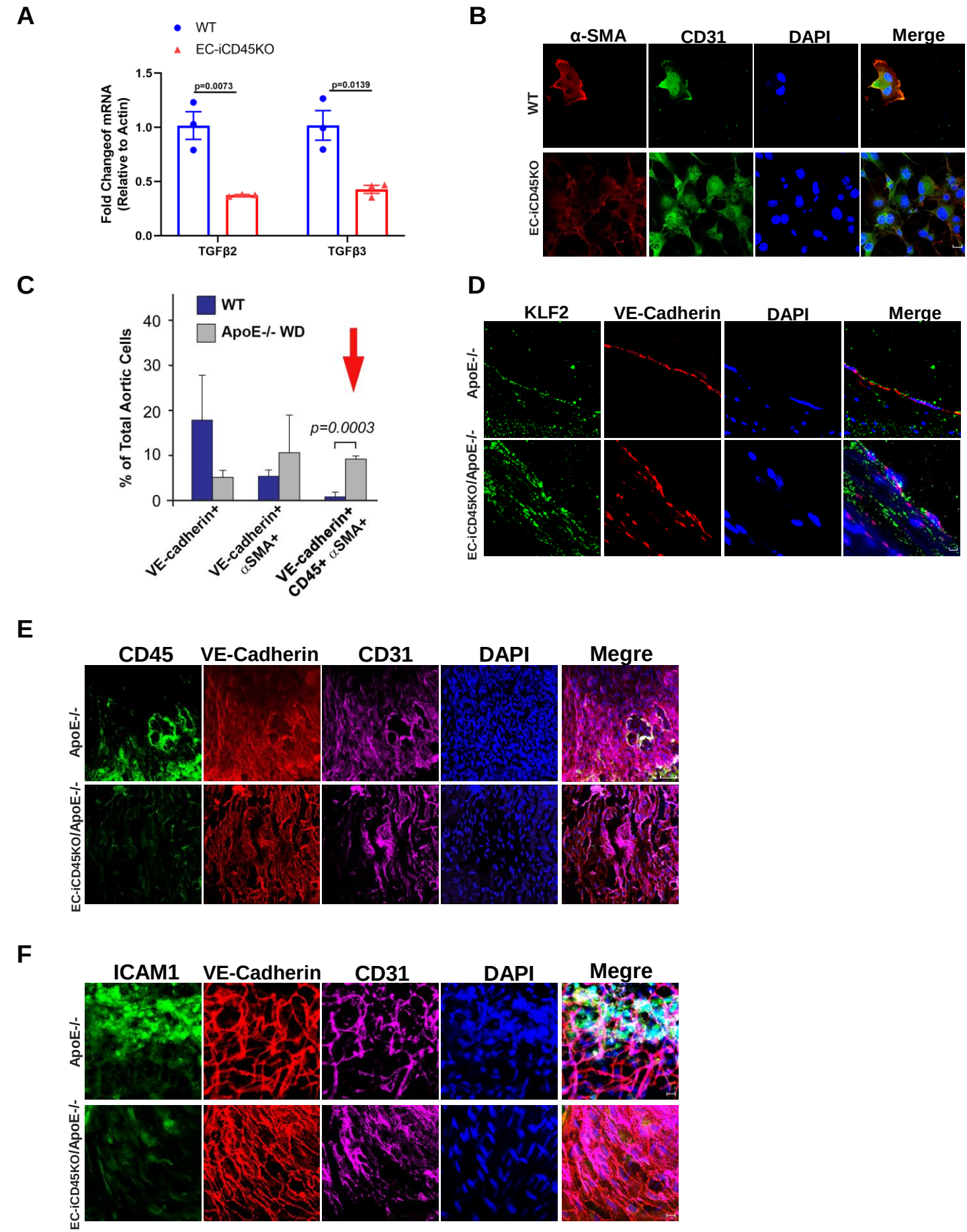
A
WT
EC-iCD45KO
Fold Changeof mRNA (Relative to Actin)
1.5
1.0
0.5
0.0
p=0.0073
p=0.0139
TGFβ2
TGFβ3
B
α-SMA
CD31
DAPI
Merge
WT
EC-iCD45KO
C
WT
ApoE-/- WD
% of Total Aortic Cells
40
30
20
10
0
p=0.0003
VE-cadherin+
VE-cadherin+ αSMA+
VE-cadherin+ CD45+ αSMA+
D
KLF2
VE-Cadherin
DAPI
Merge
ApoE-/-
EC-iCD45KO/ApoE-/-
E
CD45
VE-Cadherin
CD31
DAPI
Megre
ApoE-/-
EC-iCD45KO/ApoE-/-
F
ICAM1
VE-Cadherin
CD31
DAPI
Megre
ApoE-/-
EC-iCD45KO/ApoE-/-

Figure 5

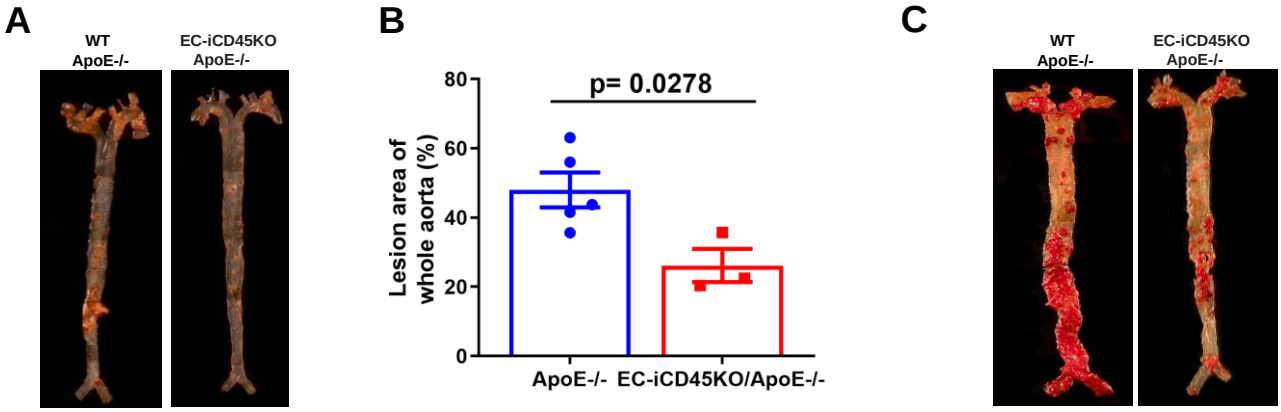
A
WT
ApoE-/-
EC-iCD45KO
ApoE-/-
B
p= 0.0278
Lesion area of whole aorta (%)
80
60
40
20
0
ApoE-/-
EC-iCD45KO/ApoE-/-
C
WT
ApoE-/-
EC-iCD45KO
ApoE-/-

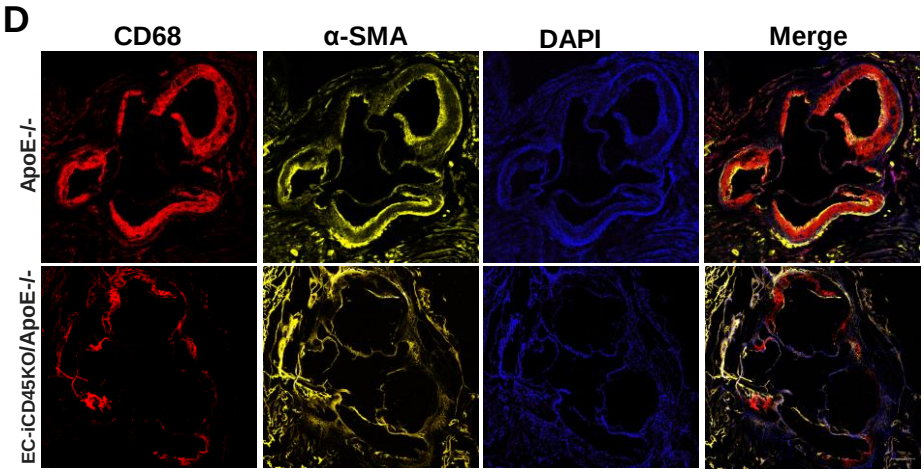
D
CD68
α-SMA
DAPI
Merge
ApoE-/-
EC-iCD45KO/ApoE-/-

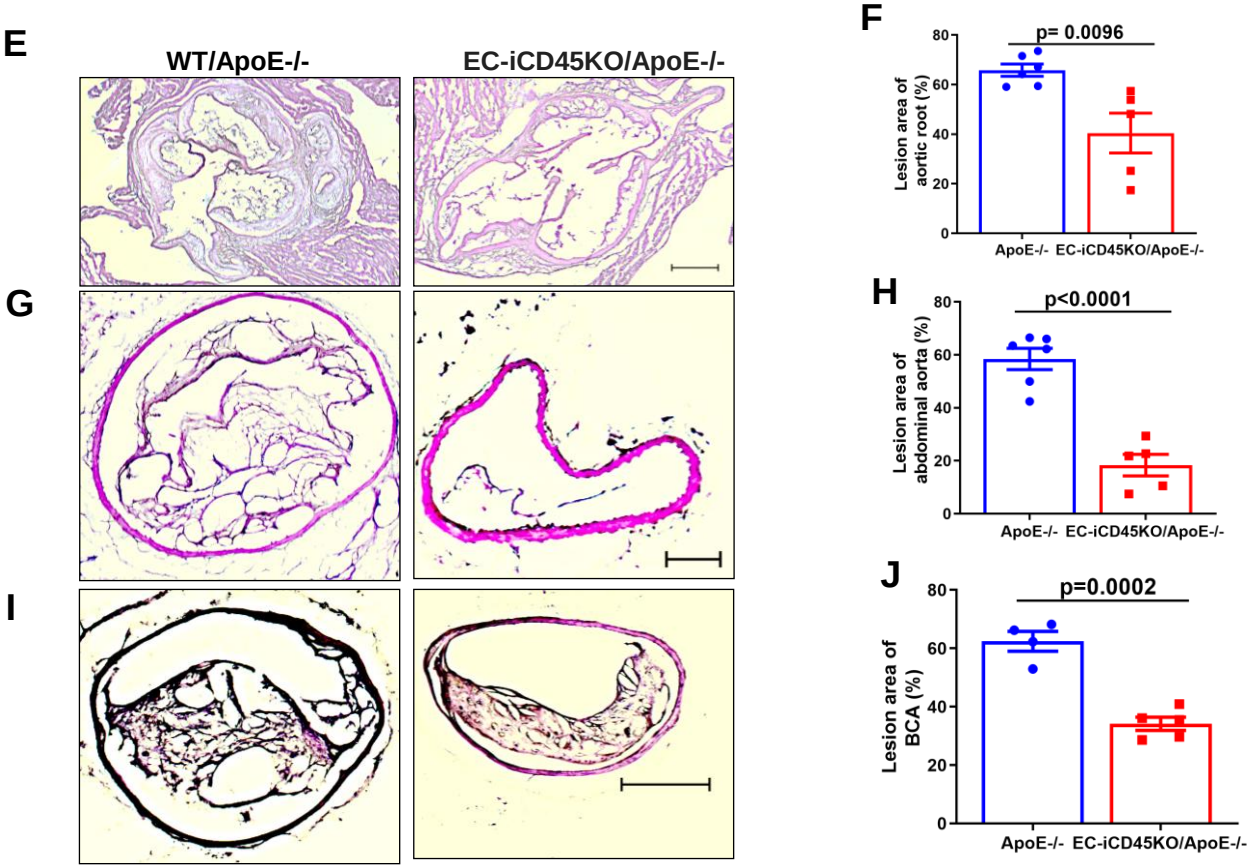
E
WT/ApoE-/-
EC-iCD45KO/ApoE-/-
G
I
F
p= 0.0096
Lesion area of aortic root (%)
80
60
40
20
0
ApoE-/-
EC-iCD45KO/ApoE-/-
H
p<0.0001
Lesion area of abdominal aorta (%)
80
60
40
20
0
ApoE-/-
EC-iCD45KO/ApoE-/-
J
p=0.0002
Lesion area of BCA (%)
80
60
40
20
0
ApoE-/-
EC-iCD45KO/ApoE-/-

Figure S1

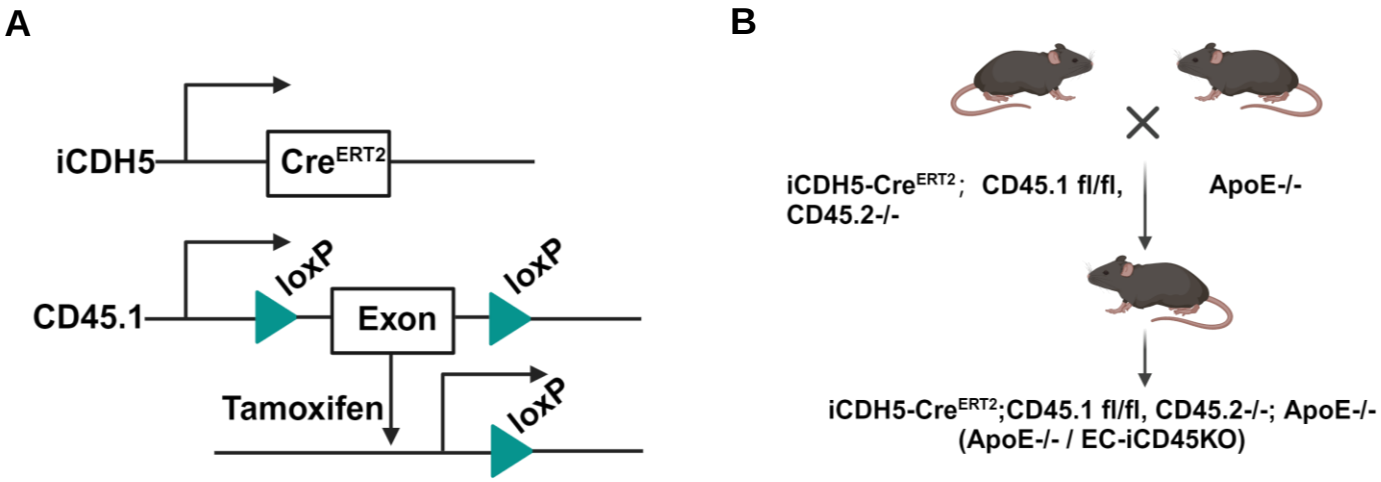
A
iCDH5
Cre^ERT2
CD45.1
loxP
Exon
loxP
Tamoxifen
loxP
B
iCDH5-Cre^ERT2; CD45.1 fl/fl, CD45.2-/-
ApoE-/-
iCDH5-Cre^ERT2;CD45.1 fl/fl, CD45.2-/-; ApoE-/-
(ApoE-/- / EC-iCD45KO)

Figure S2

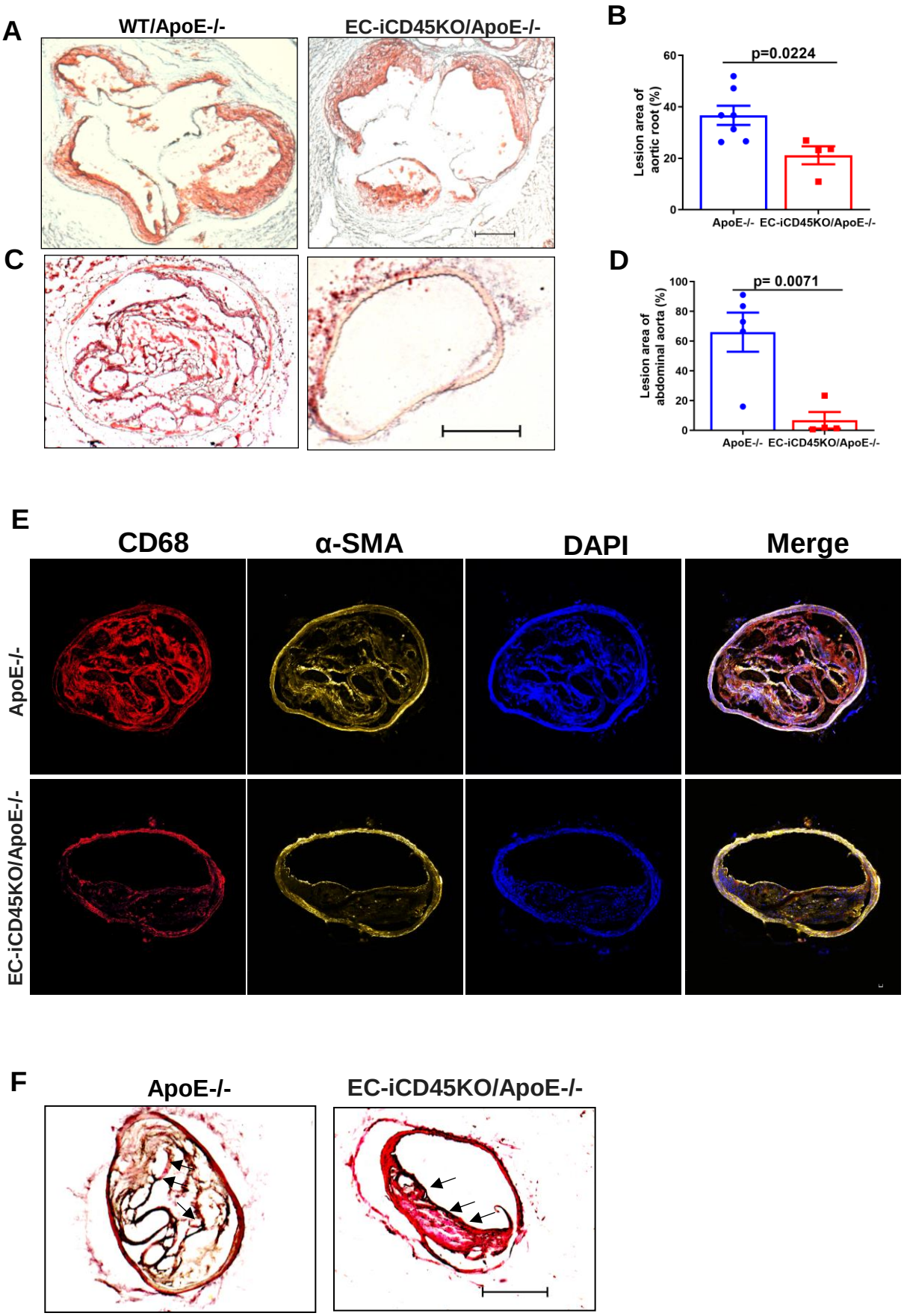
A
WT/ApoE-/-
EC-iCD45KO/ApoE-/-
B
p=0.0224
Lesion area of aortic root (%)
60
40
20
0
ApoE-/-
EC-iCD45KO/ApoE-/-
C
D
p= 0.0071
Lesion area of abdominal aorta (%)
100
80
60
40
20
0
ApoE-/-
EC-iCD45KO/ApoE-/-
E
CD68
α-SMA
DAPI
Merge
ApoE-/-
EC-iCD45KO/ApoE-/-
F
ApoE-/-
EC-iCD45KO/ApoE-/-

Figure S3

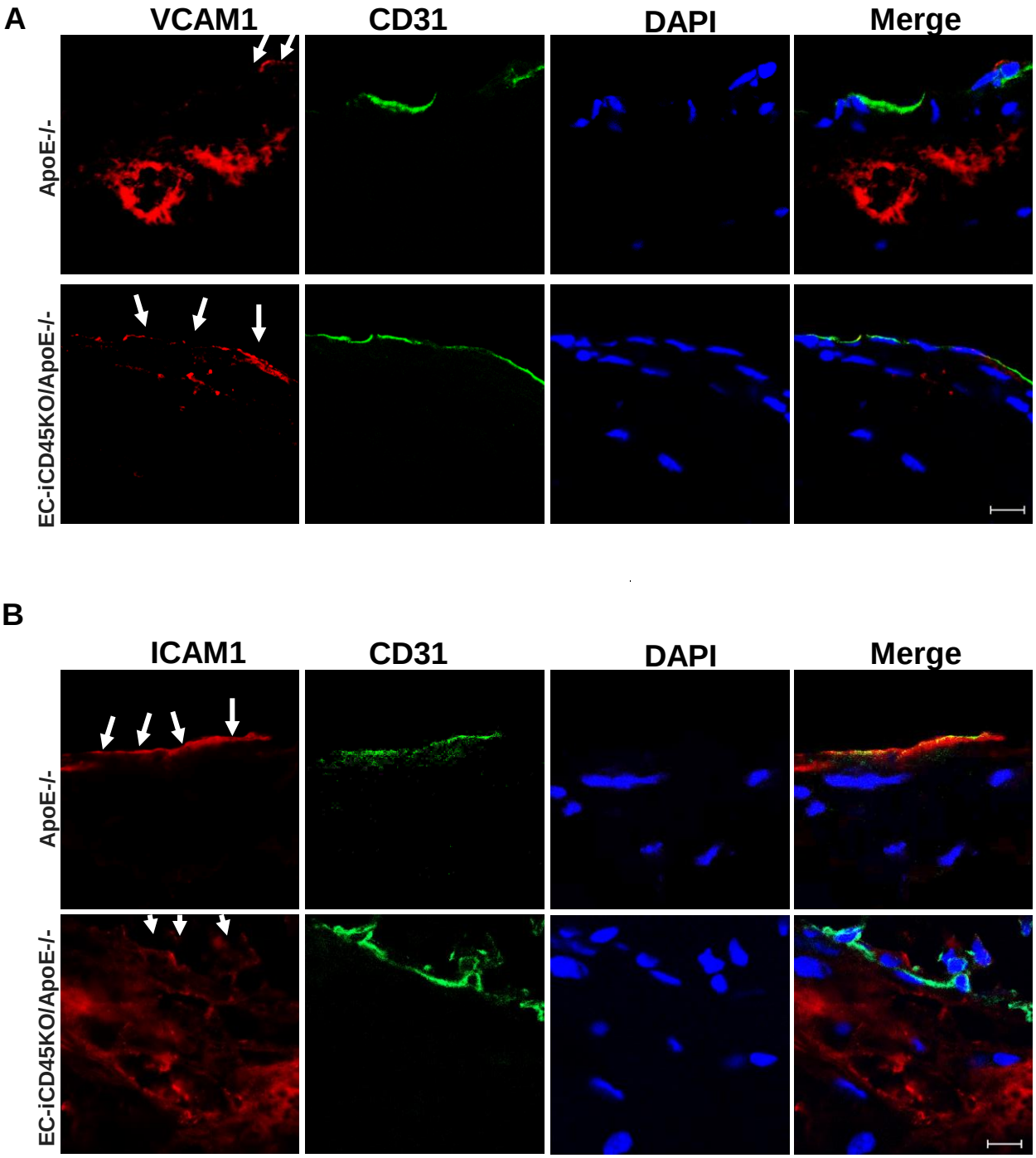
A
VCAM1
CD31
DAPI
Merge
ApoE-/-
EC-iCD45KO/ApoE-/-
B
ICAM1
CD31
DAPI
Merge
ApoE-/-
EC-iCD45KO/ApoE-/-

Figure S4

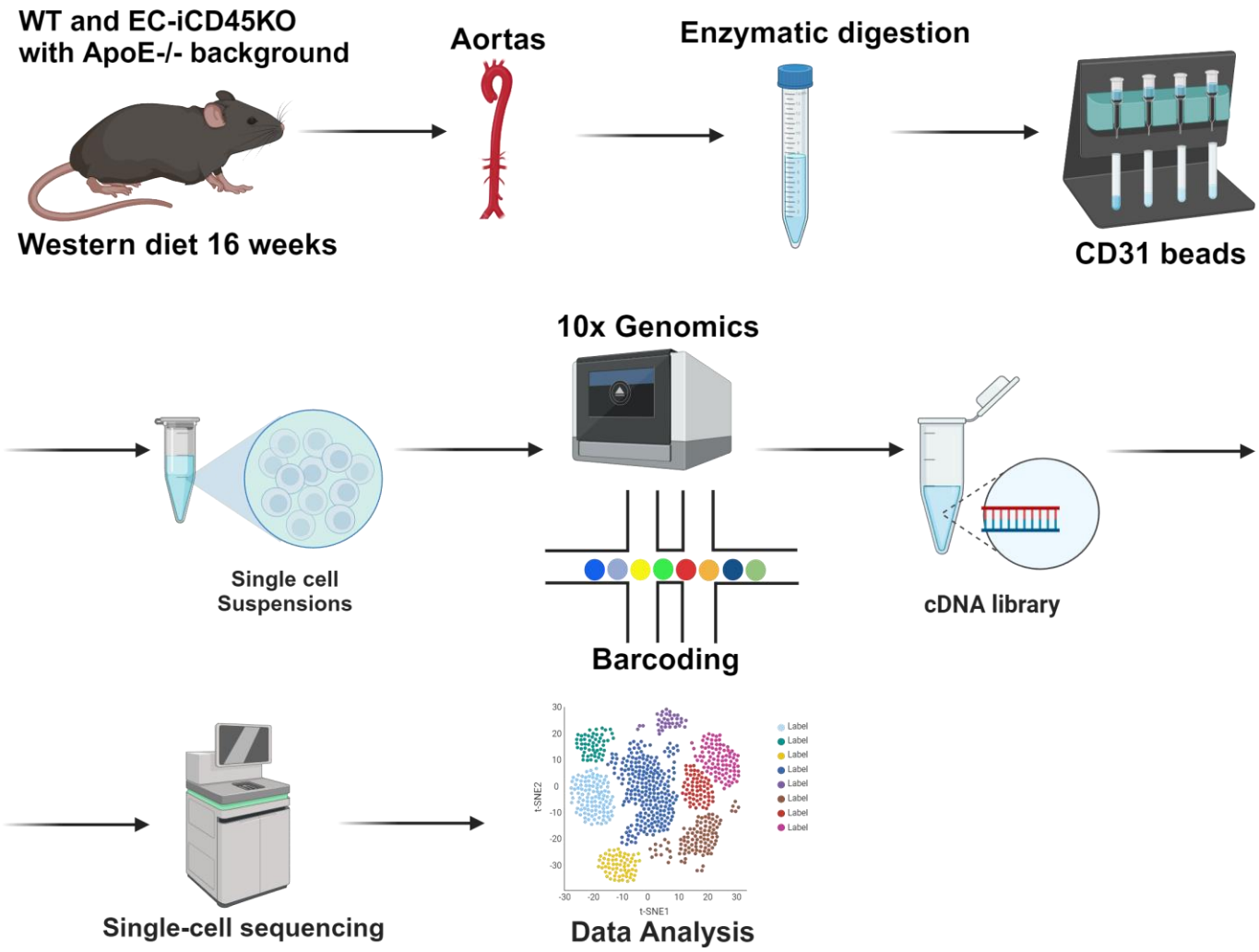
WT and EC-iCD45KO
with ApoE-/- background
Western diet 16 weeks
Aortas
Enzymatic digestion
CD31 beads
10x Genomics
Single cell
Suspensions
Barcoding
cDNA library
Single-cell sequencing
Data Analysis
t-SNE1
t-SNE2
Label

Figure S5

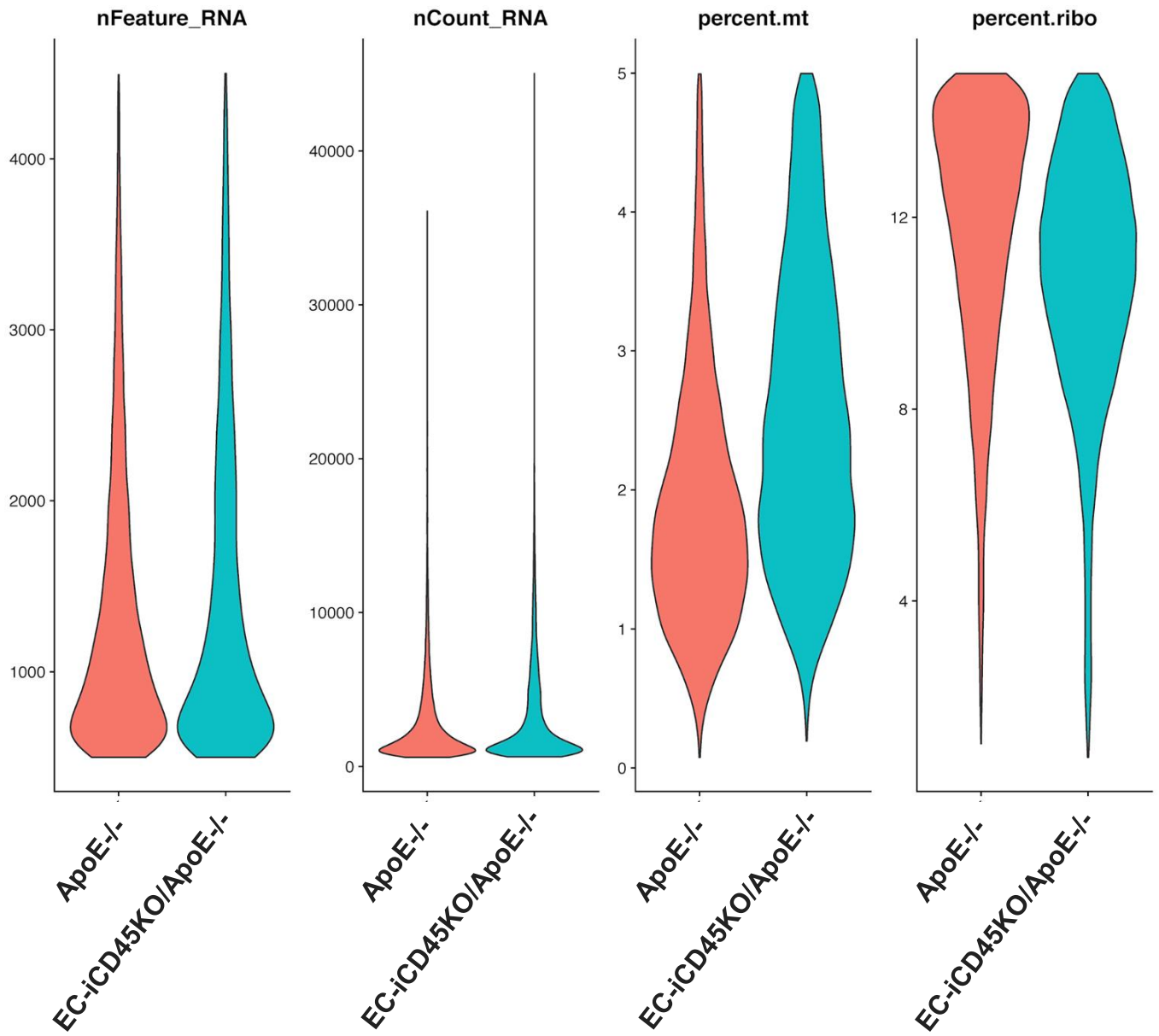

nFeature_RNA > 500 & nFeature_RNA < 4500 & percent.mt < 5 & percent.ribo < 15

Figure S6

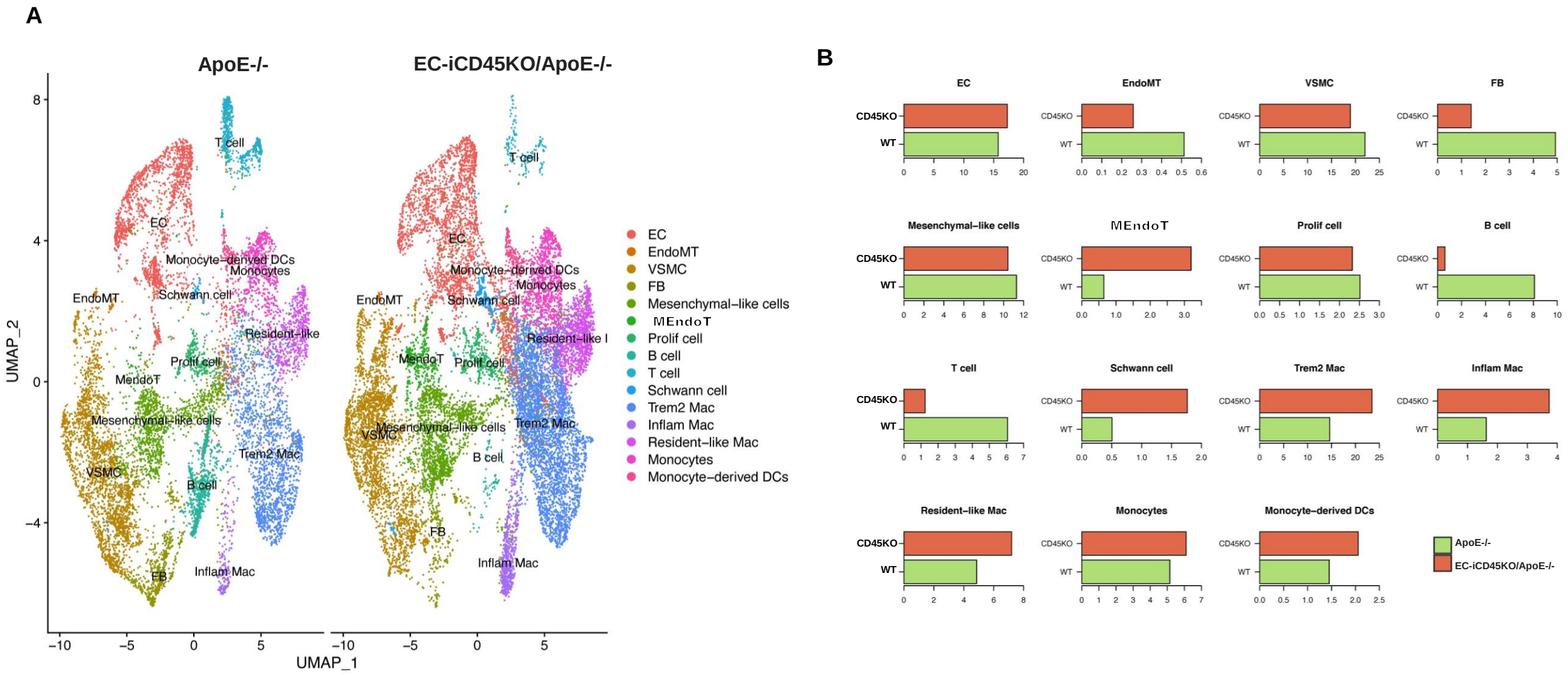
A
ApoE-/-
EC-iCD45KO/ApoE-/-
UMAP_2
UMAP_1
T cell
EC
Monocyte-derived DCs
Monocytes
EndoMT
Schwann cell
Resident-like
Prolif cell
MEndoT
Mesenchymal-like cells
VSMC
B cell
Trem2 Mac
FB
Inflam Mac
EC
EndoMT
VSMC
FB
Mesenchymal-like cells
MEndoT
Prolif cell
B cell
T cell
Schwann cell
Trem2 Mac
Inflam Mac
Resident-like Mac
Monocytes
Monocyte-derived DCs
B
EC
EndoMT
VSMC
FB
Mesenchymal-like cells
MEndoT
Prolif cell
B cell
T cell
Schwann cell
Trem2 Mac
Inflam Mac
Resident-like Mac
Monocytes
Monocyte-derived DCs
CD45KO
WT
ApoE-/-
EC-iCD45KO/ApoE-/-

Figure S7

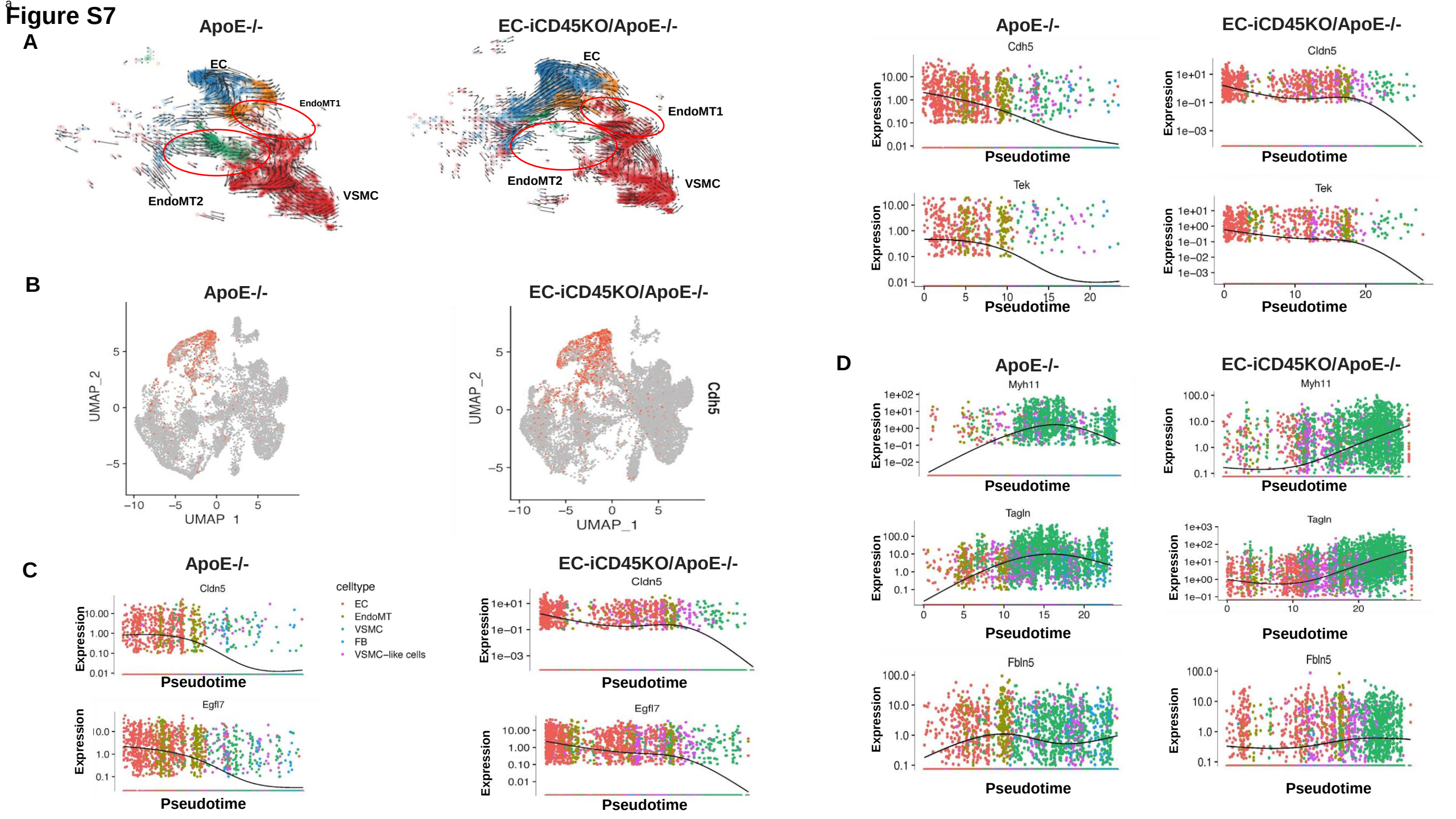
A
ApoE-/-
EC-iCD45KO/ApoE-/-
EC
EndoMT1
EndoMT2
VSMC
B
UMAP_2
UMAP_1
Cdh5
C
Cldn5
Egfl7
Expression
Pseudotime
celltype
EC
EndoMT
VSMC
FB
VSMC-like cells
D
Tek
Myh11
Tagln
Fbln5

Figure S8

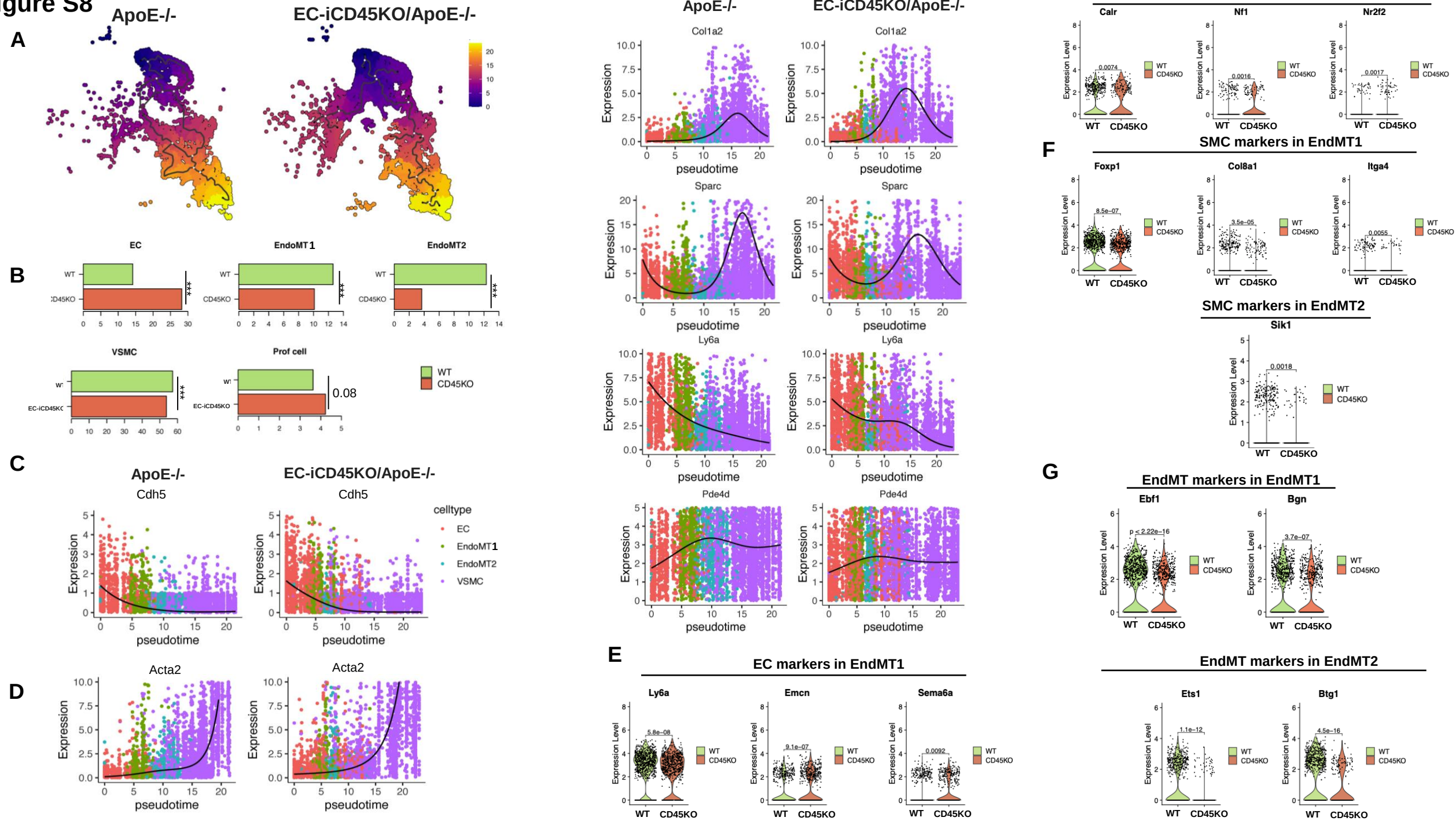
A
ApoE-/-
EC-iCD45KO/ApoE-/-
B
EC
EndoMT1
EndoMT2
VSMC
Prof cell
WT
CD45KO
EC-iCD45KO
0.08
C
ApoE-/-
EC-iCD45KO/ApoE-/-
Cdh5
celltype
EC
EndoMT1
EndoMT2
VSMC
Expression
pseudotime
D
Acta2
Col1a2
Sparc
Ly6a
Pde4d
E
EC markers in EndMT1
Ly6a
Emcn
Sema6a
F
EC markers in EndMT2
Calr
Nf1
Nr2f2
SMC markers in EndMT1
Foxp1
Col8a1
Itga4
SMC markers in EndMT2
Sik1
G
EndMT markers in EndMT1
Ebf1
Bgn
EndMT markers in EndMT2
Ets1
Btg1
Expression Level

Supplemental Materials and Methods

Animal models

In this study, all animal procedures were performed in compliance with institutional guidelines and mouse protocols were approved by the Institutional Animal Care and Use Committee (IACUC) of Boston Children's Hospital, MA, USA. Both male and female mice were used. C57BL/6 mice (stock #00664), ApoE-/- mice (stock #002052), EC-specific Cre deleter mice (iCDH5CreERT2). We crossed CD45 floxed mice with tamoxifen-inducible EC-specific Cre deleter mice (iCDH5 $CreER^{T2}$) to create an inducible EC-specific CD45 deficient mouse strain (EC-iCD45KO). We then bred EC-iCD45KO mice to the $ApoE^{-/-}$ (C57BL/6) background to obtain $ApoE^{-/-}$/EC-iCD45KO mice. For controls, we used wild-type C57BL/6 mice bearing iCDH5 CreERT2 (denoted as WT). These mice crossed to the $ApoE^{-/-}$ (C57BL/6) background to obtain control $ApoE^{-/-}$/WT ($ApoE^{-/-}$) mice. Mice were fed a Western diet (WD, D12079B, Research Diet) starting at the age of around 8 months old for 8-24 weeks. Mice were sacrificed at different time points based on the experiment.

Mouse Genotyping for CD45.1 by Polymerase Chain Reaction (PCR)

Genomic DNA was extracted from mouse tail biopsy using the DNeasy Kit (Qiagen). A triple-primer method was used for genotyping ApoE, CD45.1 and their mutants with neomycin-resistant gene inserts, respectively, using the following primer sequences: Mouse CD45 wild-type primer: 5'-'; Mouse CD45.1 mutant: 5'- -3'; Mouse CD45 common primer: 5'- -3'; ApoE forward-1: 5'- -3', ApoE forward-2: 5'- -3', and ApoE reverse: 5'- -3'. The PCR condition was as follows: jump start for 2 min at 95°C, denaturation for 1 min at 95°C, annealing for 1 min at 56 °C, and extension at 72°C for 1 min, for 40 cycles. The resulting PCR products were resolved on a 1.5 % agarose

ethidium bromide gel and the amplified bands were visualized with ultraviolet light, after which the PCR products were purified and sequence identity was confirmed by sequencing

Mouse Genotyping for CD45.2 by flow cytometry

Mouse blood was collected from the tail nick into an Eppendorf tube that contains 200µL PBS/ 10mM EDTA (anticoagulant) and stored on ice. Then, red blood cells were lysis by using red blood cell lysis buffer (Millipore Sigma Cat# 11814389001), and cell pellets were spun down. We then added 500µL buffer (2%HBSS without phenol red + 0.1% BSA + 0.02% Na azide) to wash RBC lysis buffer from cells and spun down. Next, remove the supernatant from the pellets. Cell pellets were resuspended in FACS buffer with Trustain (anti-mouse CD16/32) from BioLegend, anti-mouse CD45.1-PE (BioLegend) and CD45.2-FITC (BioLegend) at 4°C, 30 min before flow cytometry analysis using BD instrument.

MAEC isolation

To isolate mouse aortic endothelial cells (MAECs), aortas were collected and washed twice with PBS at 4 °C and then carefully stripped of fat and connective tissue. The aortas were cut into 3 mm long sections, and segments were put on Matrigel-coated (Corning) plate with EC medium. After 4 days, vascular networks were visible under the light microscope and tissue segments were removed. ECs were detached, spun down and cultured in fresh EC medium. The identity of isolated ECs was confirmed by immunofluorescent staining using EC markers CD31. A full list of reagents including antibodies and primers is included in the supplementary information (Supplementary Data file 4). Cultured MAECs were treated with 5 µM tamoxifen for 3 days to induce the deletion of CD45 gene from EC-iCD45KO/ApoE$^{-/-}$ mice, MAECs isolated from ApoE$^{-/-}$ mice as controls

(without tamoxifen treatment). Cells were treated with 100 μg/mL oxLDL or 10ng/mL TGFβ1 at different times as indicated while maintaining 2 μM tamoxifen in the culture medium.

Flow cytometry analysis

We applied the triple-label flow cytometric method we developed for mitral valve analyses to total aortic ECs from age and gender-matched wild-type (WT) and ApoE$^{-/-}$ mice fed a WD for 16-20 weeks. As ApoE$^{-/-}$ mice fed a normal diet also develop lesions, albeit at a slower rate compared to WD-fed ApoE$^{-/-}$ mice, we chose to use WT mice that were fed a normal chow as our true negative control for EndoMT occurrence to rule out the potential effect of high cholesterol content in WD-fed mice and lesion development in normal chow-fed ApoE$^{-/-}$ mice. Blood was thoroughly flushed from aortas to enrich vessel wall-localized cells. Antibodies were rat anti-mouse CD45 (BD Biosciences #564590), anti-VE-cadherin-FITC(), anti-CD45-CF647(), anti-FGFR1-PE(), and rabbit anti-human VE-cadherin (ABD Serotec #AHP628Z) coupled to APC using the LYNX Rapid APC Antibody Conjugation Kit (ABD Serotec #LNK031APC) as well as rabbit anti-human α-SMA-PE (Abcam #ab209478) with isotype-matched control IgGs and matching fluorescent tags. Antibodies were authenticated by showing binding to murine CD45, VE-cadherin, and α-SMA, respectively, and using appropriate positive and negative controls.

Supplement Table 1 : Major Resources Table

Antibodies

Target antigen	Vendor or Source	Catalog #	Working concentration
Primary Antibodies			
Mouse VE-Cadherin Antibody	R & D systems	AF1002	1:50(IF)
Anti-Klf2 Antibody (Rabbit Polyclonal Antibody	EMD Millipore	09-820	1:200(IF)
Mouse monoclonal anti-CD68	Santa Cruz Biotechnology	Sc20060	1:200(IF)
Anti-Actin, α-Smooth Muscle - Cy3™ antibody, Mouse monoclonal α-SMA	Sigma-Aldrich	C6198	1:200(IF)
Rat-anti Mouse CD31	BD Pharmingen	550274	1:50(IF)
Mose Anti-CD45	Santa Cruz Biotechnology	Sc-28369	1:200
Mouse monoclonal ICAM-1	Santa Cruz Biotechnology	Sc8439	1:200(IF)
Mouse monoclonal VCAM-1	Santa Cruz Biotechnology	sc13160	1:70(IF)
Alexa Fluor Conjugated Second Antibodies		REF	2mg/ML
Goat anti-rabbit 647	Invitrogen	A-21244	1:200(IF)
Goat anti-rat 647	Invitrogen	A-21247	1:200(IF)
Donkey anti-mouse 594	Invitrogen	A-21203	1:200(IF)
Donkey anti-rabbit 594	Invitrogen	A-21207	1:150(IF)
Donkey anti-rat 594	Invitrogen	A-21209	1:150(IF, Flow)
Donkey anti-rat 488	Invitrogen	A-21208	1:200(IF)
Donkey anti-mouse 488	Invitrogen	A-21202	1:150(IF, Flow)
Donkey anti-rabbit 488	Invitrogen	A-21206	1:150(IF, Flow)
IF			
Donkey anti-rabbit 647	Invitrogen	A31573	1:200(IF) Lot:2674379

Donkey anti-goat 594	Invitrogen	A11058	1:200(IF)
Donkey anti-Rat 647	Invitrogen	A21247	1:200(IF)
Donkey anti-mouse 647	Invitrogen	A31571	1:200(IF)

Reagents

Description	Source / Repository	Catalog #
Oil Red O (ORO)	Thermo Scientific	Cat# A12989
Hematoxylin and Eosin stain kit	Vector Laboratories	Cat# H-3502
Propylene glycol	VWR	0575
Oxidized LDL (ox-LDL)	Athens Research and Technology	Cat#12-16-120412-ox
Low Density Lipoprotein from Human Plasma, oxidized, DiI conjugate (DiI-OxLDL)	ThermoFisher Scientific	Cat# L34358
TopFluor Cholesterol	Avanti Polar Lipids,Inc	Cat# 810255p
SlowFade mount with DAPI	Invitrogen	Cat# 1896320
Protein inhibitor cocktail	**cOmplete ™**	REF:11836170001
Isopropanol, molecular biology grade	ThermoFisher Scientific	Cat# T036181000CS

Qiagen RNeasy Mini Kit	Qiagen	Cat# 74104
RNase-free DNAse Set	Qiagen	Cat# 79254

HiScript II One Step qRT-PCR SYBR Green Kit	Vazyme	Q221-01
SYPR Green qPCR Master Mix reagent	Vazyme	Cat# Q712
Fluoroshield	R & D Systems	F6812
Ciprofloxacin Hydrochloride	TCI AMERICA	C2227
Triton™ X-100 Surfactant	MilliporeSigma	TX15681
Matrigel Matrix	Corning	REF#356237
CD31 MicroBeads (Mouse)	Miltenyi Biotec	Cat# 130-097-418
Collagenase type I	Gibco by Life technologies	Ref 17100-017
Collagenase type IV	Gibco by Life technologies	Ref 17104-019
Liberase	Roche	Cat# 05401127001
GEM Single Cell 3'GEM Kit v3.1	10X Genomics	PN-1000123
GEM Single Cell 3'Library Kit v3.1	10X Genomics	PN-1000157
GEM Single Cell 3'Gel Bead Kit v3.1	10X Genomics	PN-1000122
Dynabeads™ MyOne™ SILANE	10X Genomics	PN-2000048
GEM Chip G Single Cell Kit, 48rxns	10X Genomics	PN-1000120

Single Index Kit T Set A, 96 rxns	10X Genomics	PN-1000213

Oligonucleotides

Description	Source / Repository	Catalog #
TGFβ2	This study	N/A
Forward: 5'- GGACCCTACTCTGTCTGTGG -3' Reverse: 5'- AGCCATGGAGTAGACATCCG -3'		
TGFβ3	This study	N/A
Forward: 5'- GACATCCCTTCCACCCAAGA-3' Reverse: 5'- CAGGAGGAATGGTGTGGACT -3'		
Beta-actin	This study	N/A
Forward: 5'- TTACTGCTCTGGCTCCTAGCA-3' Reverse: 5'-CCACCGATCCACACAGAGTAC-3'		

Software and Algorithms

Description	Persistent ID / URL
Image J	NIH website: https://imagej.nih.gov/ij/
GraphPad Prism	GraphPad software company: https://www.graphpad.com/scientificsoftware/prism/
Zeiss Zen lite	https://www.zeiss.com/microscopy/us/products/microscope-software/zen-lite.html
Image J	NIH website: https://imagej.nih.gov/ij/

GraphPad Prism	GraphPad software company: https://www.graphpad.com/scientificsoftware/prism/